Renewable and Sustainable Energy Reviews 25 (2013) 793–813

Contents lists available at SciVerse ScienceDirect

Renewable and Sustainable Energy Reviews

journal homepage: www.elsevier.com/locate/rser

MPPT techniques for photovoltaic applications

Mohamed A. Eltawil [a,c,*], Zhengming Zhao [b]

[a] Agricultural Systems Engineering Department, College of Agriculture and Food Sciences, King Faisal University, P.O. 380, Al-Ahsa 31982, Saudi Arabia
[b] The State Key Laboratory of Power System, Department of Electrical Engineering, Tsinghua University, Beijing 100084, China
[c] Agricultural Engineering Department, Faculty of Agriculture, Kafrelsheikh University, Box 33516, Egypt

ARTICLE INFO

Article history:
Received 23 February 2013
Accepted 7 May 2013
Available online 26 June 2013

Keywords:
MPPT
PV
Tracking factor for MPP
Fuzzy logic controller
Incremental conductance
Perturb and observe
Neural network

ABSTRACT

The photovoltaic (PV) system is one of the renewable energies that attract the attention of researchers in the recent decades. The PV generators exhibit nonlinear *I–V* and *P–V* characteristics. The maximum power produced varies with both irradiance and temperature. Since the conversion efficiency of PV arrays is very low, it requires maximum power point tracking (MPPT) control techniques. The maximum power point tracking (MPPT) is the automatic control algorithm to adjust the power interfaces and achieve the greatest possible power harvest, during moment to moment variations of light level, shading, temperature, and photovoltaic module characteristics. The purpose of the MPPT is to adjust the solar operating voltage close to the MPP under changing atmospheric conditions. It has become an essential component to evaluate the design performance of PV power systems. This investigation aims to assess different MPPT techniques, provide background knowledge, implementation topology, grid interconnection of PV and solar microinverter requirements presented in the literature, doing depth comparisons between them with a brief discussion. The MPPT merits, demerits and classification, which can be used as a reference for future research related to optimizing the solar power generation, are also discussed. Conventional methods are easy to implement but they suffer from oscillations at MPP and tracking speed is less due to fixed perturb step. Intelligent methods are efficient; oscillations are lesser at MPP in steady state and tracked quickly in comparison to conventional methods.

Contents

1. Introduction

The continuous growth of energy demand from all around the world has urged the society to seek for alternative energies due to the depletion of conventional energy resources and their undesirable impact on environment. Among the available alternative energies, photovoltaic (PV) energy is one of the most promising renewable energies.

PV energy is clean, simple in design requiring very little maintenance and their biggest advantage being their construction as stand-alone systems to give outputs from microwatts to megawatts. Hence they are used for power source, water pumping, remote buildings, solar home systems, communications, satellites and space vehicles, reverse osmosis plants, and for even megawatt scale power plants. With such a vast array of applications, the demand for photovoltaics is increasing every year [1].

However, there are two main drawbacks of PV system, namely the high installation cost and the low conversion efficiency of PV modules which is only in the range of 9–17%. Besides that, PV characteristics are nonlinear and weather dependent.

Baltas et al. [2] suggested that, instead of tracking the sun continuously, an array could be moved after a time interval such

* Corresponding author at: Agricultural Engineering Department, Kafrelsheikh University, Box 33516, Egypt. Tel./fax: +20 47 9102930.
E-mail addresses: eltawil69@yahoo.co.in, mohamed.eltawil@agr.kfs.edu.eg (M.A. Eltawil).

1364-0321/$ - see front matter
http://dx.doi.org/10.1016/j.rser.2013.05.022

that it was directed to the middle of the sun trajectory during the next time interval. For south facing fixed tilted array, it has been found that, the two step tracking configuration produced about 95% of energy to that of continuously tracking system around solar noon. It was also observed that, the tilt of a south facing array be optimized to provide more energy during certain months of the year. A solar PV system could be designed for its optimum output using the contour plots constructed on the basis of monthly energy outputs for different panel tilt angles.

Chander et al. [3] observed that about 36% higher annual energy output could be obtained with a dual axis tracking as compared to fixed latitude tilted PV system. They developed a theoretical model to estimate the annual PV energy output from the array at a given location for any arbitrary orientation, and its results was comparable with experimental results. Ramamurthy et al. [4] observed that, a single tracking of PV panel yielded 25% more energy per day and two axis tracking 35% more energy per day compared to panels at fixed tilt throughout the day.

Snyman and Enslin [5] studied a novel technique for the improvement of power conversion efficiencies in PV systems with battery backup. This technique embraces a maximum power point tracker (MPPT) in series with the PV array and the battery in such a way that the array current flows through the MPPT and the battery. The current rating of the MPPT must be at least equal to the short circuit of the array and the voltage rating must be at least equal to the open circuit voltage minus the battery voltage. This technique enables PV system designers to use the highest possible array voltage and the smallest possible battery (reduction battery cost).

2. Maximum power point tracker (MPPT)

The MPPT is described as circuitry associated with utility-interactive inverters (and some larger stand-alone) that continuously adjust the dc operating point to obtain the maximum power available from a PV array at any given time.

Despite all the advantages presented by the generation of energy through the use of PVs, the efficiency of energy conversion is currently low and the initial cost for its implementation is still considered high, and thus it becomes necessary to use techniques to extract the maximum power from these panels, in order to achieve maximum efficiency in operation. It should be noted that there is only one maximum power point (MPP), and this varies according to climatic and irradiation conditions.

The photovoltaic power characteristics is nonlinear, as shown in Fig. 1, which vary with the level of solar irradiation and temperature, which make the extraction of maximum power a complex task, considering load variations [6]. To overcome this problem, several methods for extracting the maximum power have been proposed in literature [7–15].

A PV array under constant uniform irradiance has a current–voltage (*I–V*) characteristic like that shown in Fig. 2. There is a unique point on the curve, called the maximum power point (MPP), at which the array operates with maximum efficiency and produces maximum output power. When a PV array is directly connected to a load (a so-called 'direct-coupled' system), the system's operating point will be at the intersection of the *I–V* curve of the PV array and load line shown in Fig. 2. In general, this operating point is not at the PV array's MPP, which can be clearly seen in the figure. Thus, in a direct-coupled system, the PV array must usually be oversized to ensure that the load's power requirements can be supplied. This leads to an overly expensive system.

A maximum power point tracker is a device employing a microprocessor to achieve both function of maximum power output and tracking by sampling the power output of the array at frequent intervals (usually 30 ms). It compares each new value of the array power output with the previous value. If the power output has increased then the array voltage is stepped up in the same direction otherwise it remains at the original position.

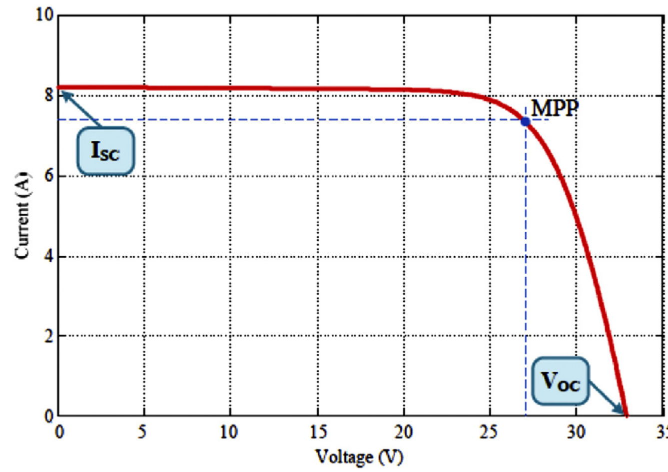


Fig. 1. PV current versus voltage characteristic.

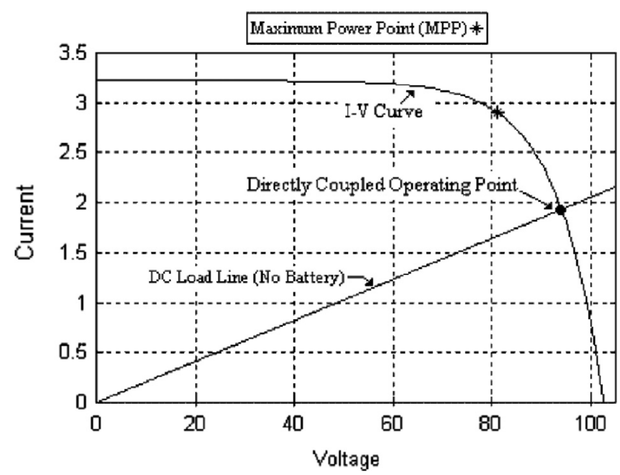


Fig. 2. Typical current–voltage curve for a PV array.

Owing to changes in the solar radiation energy and the cell operating temperature, the output power of a solar array is not constant at all times. To overcome this problem, a switch-mode power converter, called a maximum power point tracker (MPPT), can be used to maintain the PV array's operating point at the MPP [16–18]. Therefore, works to solve the problems on maximum power point tracking (MPPT) have always been a hot topic for PV array utilization systems. The MPPT does this by controlling the PV array's voltage or current independently of those of the load. If properly controlled by an MPPT algorithm, the MPPT can locate and track the MPP of the PV array. However, the location of the MPP in the *I–V* plane is not known a priori. It must be located, either through model calculations or by a search algorithm. The situation is further complicated by the fact that the MPP depends in a nonlinear way on irradiance and temperature, as illustrated in Fig. 3. Fig. 3(a) shows a main of PV *I–V* curves under increasing irradiance, but at constant temperature, and Fig. 3 (b) shows *I–V* curves at the same irradiance values, but a higher temperature. Note the change in the array voltage at which the MPP occurs.

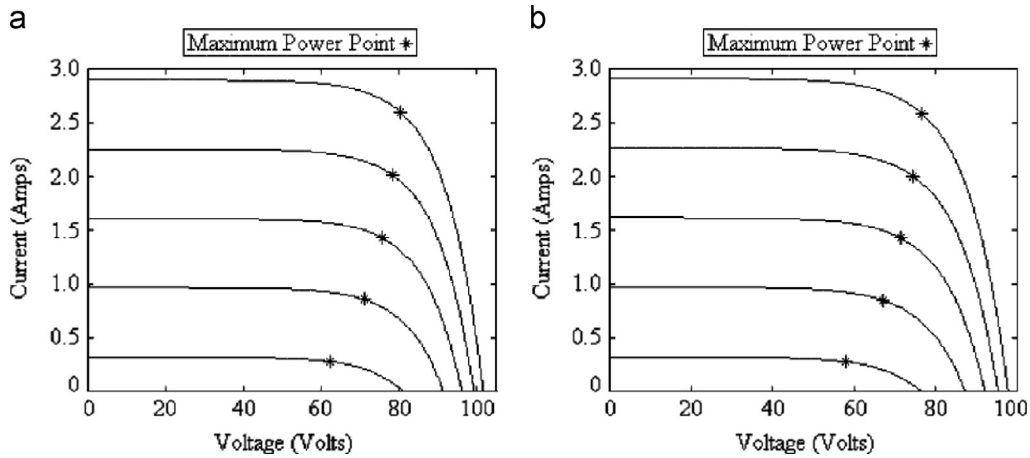


Fig. 3. (a) PV array voltage–current at 40 °C at different irradiance levels and (b) PV array voltage–current at 50 °C at different irradiance levels.

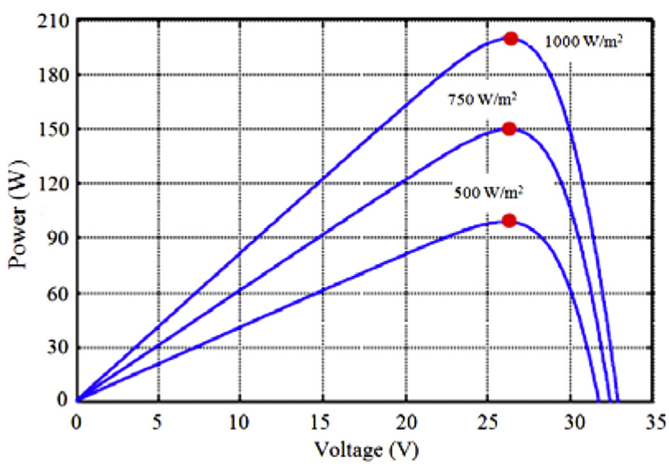


Fig. 4. PV power characteristic for different irradiation levels.

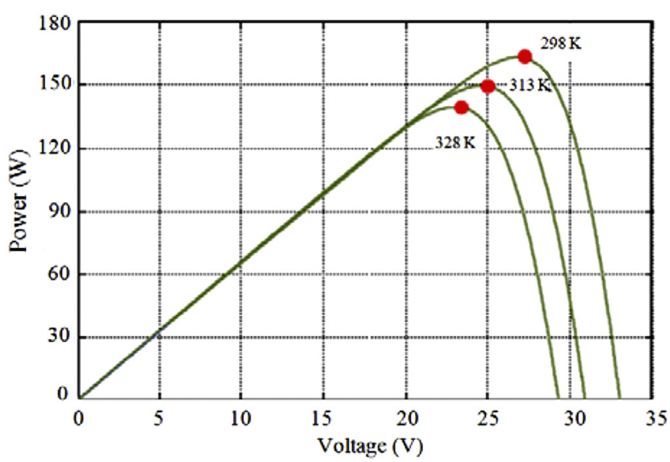


Fig. 5. PV power characteristic for different temperature levels.

Table 1
Electrical parameters of the PV.

Maximum power	P_{max}=200 Wp
Voltage at MPP	V_{MPP}=26.3 V
Current at MPP	I_{MPP}=7.61 A
Open circuit voltage	V_{OC}=32.9 V
Short circuit current	I_{SC}=8.21 A
Temperature coefficient of I_{SC}	$\alpha=3.18\times10^{-3}$ A/°C

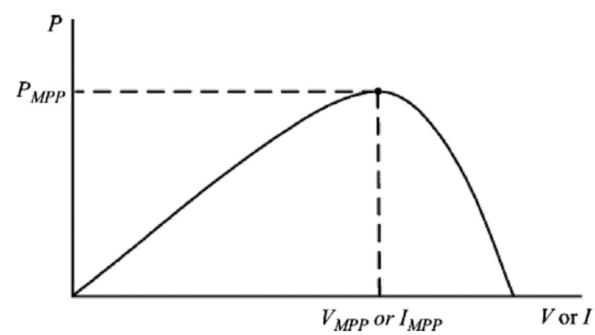


Fig. 6. Characteristic PV array power curve.

Figs. 4 and 5 show the power characteristics of the analyzed PV, considering the same temperature and solar irradiation, respectively. The curves show clearly nonlinear characteristics and they are strongly influenced by climate changes [6]. The main PV electrical parameters used are summarized in Table 1.

There are many MPPT methods have been developed and implemented. The methods vary in complexity, sensors required, convergence speed, cost, range of effectiveness, implementation hardware, popularity, and in other respects. They range from the almost obvious (but not necessarily ineffective) to the most creative (not necessarily most effective). In fact, so many methods have been developed that it has become difficult to adequately determine which method, newly proposed or existing, is most appropriate for a given PV system.

2.1. Problem overview

Fig. 6 shows the characteristic power curve for a PV array. The problem considered by MPPT techniques is to automatically find the voltage *VMPP* or current *IMPP* at which a PV array should operate to obtain the maximum power output *PMPP* under a given temperature and irradiance.

The MPP voltage has a complicated dependence on both irradiance and temperature and the point is usually found by the MPP tracker by a trial and error algorithm. The irradiance and hence the current can vary rapidly as the sun goes behind or comes out from clouds but the module temperature varies slowly.

It is noted that under partial shading conditions, in some cases it is possible to have multiple local maxima, but overall there is still only one true MPP. Most techniques respond to changes in both irradiance and temperature, but some are specifically more

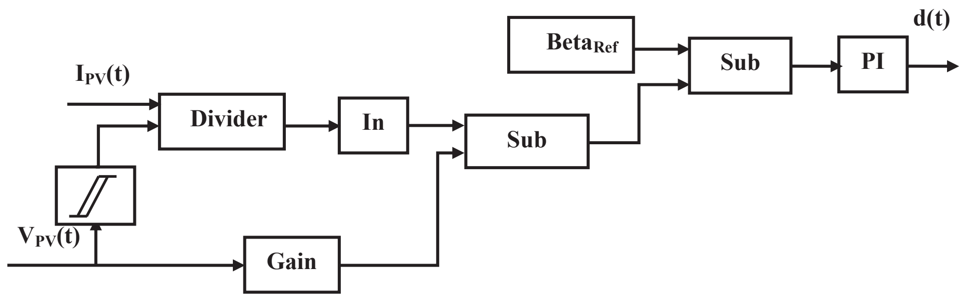


Fig. 7. Implementation of the Beta method.

useful if temperature is approximately constant. Most techniques would automatically respond to changes in the array due to aging, though some are open-loop and would require periodic fine-tuning. In our context, the array will typically be connected to a power converter that can vary the current coming from the PV array.

2.2. MPPT techniques

The different techniques of MPPT are described briefly as follows:

(i) **Fixed duty cycle**
The fixed duty cycle represents the simplest of the methods and it does not require any feedback, where the load impedance is adjusted only once for the maximum power point and it is not adjusted again.

(ii) **Beta method**
The Beta method is the approximation of the point of maximum power through the equation of an intermediate variable β.

$$\beta = \ln\left(\frac{I_{PV}}{V_{PV}}\right) - cV_{PV} \quad (1)$$

where $c = q/(\sigma$ K.T.Ns) is a constant that depends on the electron charge, the quality factor of the junction panel, the Boltzmann constant, temperature and amount of photovoltaic cells in series [19]. As the operating conditions change, the value of β at the optimum point remains almost constant. Thus, β can be continuously calculated using the voltage and current of the panel and inserted on a conventional closed loop with constant reference, as shown in Fig. 7.

(iii) **Hill climbing/perturb and observe**
There are several authors focus their work on hill climbing [20–25], while others focus on perturb and observe (P&O) [26–36] methods. Hill climbing involves a perturbation in the duty ratio of the power converter, and P&O a perturbation in the operating voltage of the PV array. In the case of a PV array connected to a power converter, perturbing the duty ratio of power converter perturbs the PV array current and consequently perturbs the PV array voltage. Hill climbing and P&O methods are different ways to envision the same fundamental method.
The perturb and observe (P&O) algorithm is the most commonly used in practice because of its ease of implementation [37]. Fig. 8 shows the flow chart of P&O method. It perturbs the PV array's terminal voltage periodically, and then it compares the PV output power with that of the previous cycle of perturbation [38–41].
As shown in Fig. 8, when PV power and PV voltage increase at the same time and vice versa, a perturbation step size, ΔD will be added to the duty cycle, D to generate the next cycle of perturbation in order to force the operating point moving towards the MPP. When PV power increases and PV voltage decreases and vice versa, the perturbation step will be subtracted for the next cycle of perturbation [42]. This process will be carried on continuously until MPP is reached.
It should be noted that, the system will oscillate around the MPP throughout this process, and this will result in loss of energy. Therefore, reducing the perturbation step size will minimize these oscillations but it slows down the MPP tracking system [40,41].
Fig. 9 shows the configurations of MPPT algorithms in Simulink according to the flow chart of P&O method explained in Fig. 8.
The most basic form of the P&O algorithm operates as follows. Consider Fig. 10, which shows a family of PV array power curves as a function of voltage (*P–V* curves), at different irradiance (G) levels, for uniform irradiance and constant temperature. As previously described, these curves have global maxima at the MPP. Assume the PV array to be operating at point A in Fig. 10, which is far from the MPP. In the P&O algorithm, the operating voltage of the PV array is perturbed by a small increment, and the resulting change in power, ΔP, is measured. If ΔP is positive, then the perturbation of the operating voltage moved the PV array's operating point closer to the MPP. Thus, further voltage perturbations in the same direction (that is, with the same algebraic sign) should move the operating point toward the MPP. If ΔP is negative, the system operating point has moved away from the MPP, and the algebraic sign of the perturbation should be reversed to move back toward the MPP.
The advantages of this algorithm, as stated before, are simplicity and ease of implementation. However, P&O has limitations that reduce its MPPT efficiency. One such limitation is that as the amount of sunlight decreases, the *P–V* curve flattens out, as seen in Fig. 10. This makes it difficult for the MPPT to discern the location of the MPP, owing to the small change in power with respect to the perturbation of the voltage. Another fundamental drawback of P&O is that it cannot determine when it has actually reached the MPP. Instead, it oscillates around the MPP, changing the sign of the perturbation after each ΔP measurement. Also, it has been shown that P&O can exhibit erratic behavior under rapidly changing irradiance levels [38]. Fig. 11 shows a close-up view of the solar array *P–V* characteristic near the MPP. Consider the case in which the irradiance is such that it generates *P–V* curve 1 in Fig. 11. The MPPT is oscillating around the MPP from point B to A to C to A and so on. Then, assume the irradiance increases and the *P–V* curve of the array moves to curve 2. If, during the rapid increase in solar irradiance and output power, the MPPT was perturbing the operating point from point A to point B, the MPPT would actually move from A to D. As seen in Fig. 11, this result in a positive ΔP, and the MPPT will continue perturbing in the same

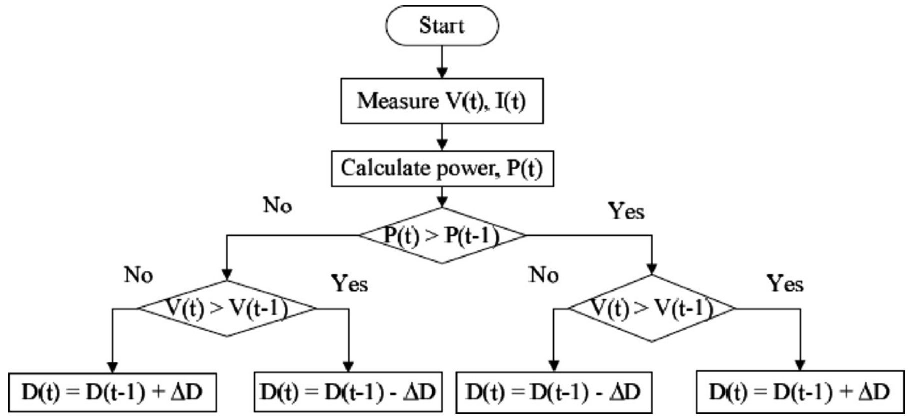


Fig. 8. Flow chart of perturb and observe method (P&O) [38].

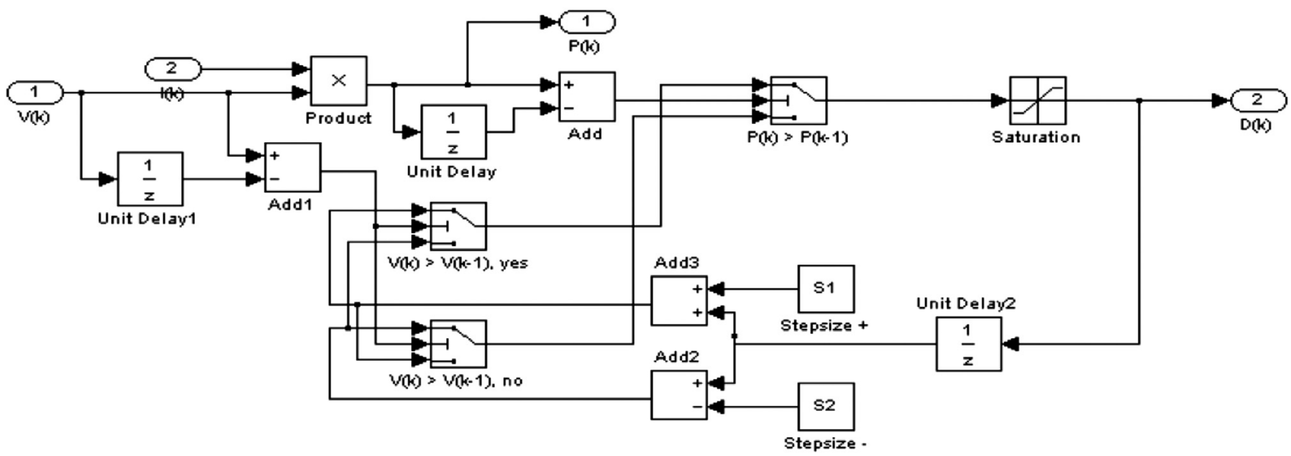


Fig. 9. Configurations of MPPT algorithms in Simulink for perturb and observe (P&O) MPPT algorithm [21].

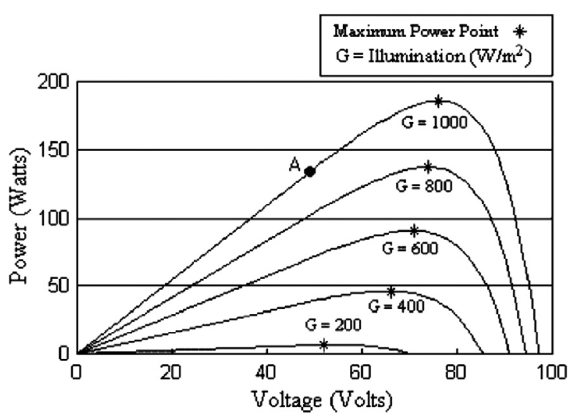


Fig. 10. Photovoltaic array power–voltage relationship.

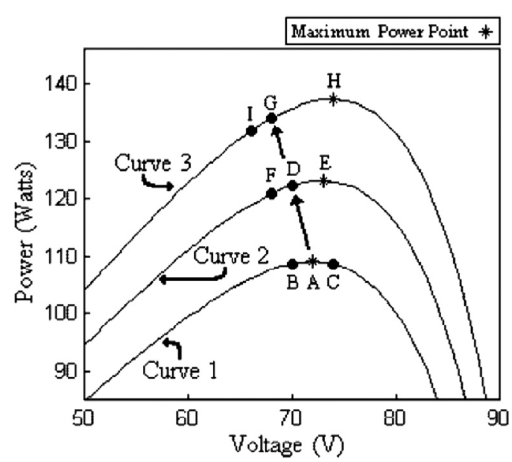


Fig. 11. Illustration of erratic behavior of P&O under rapidly increasing irradiance [18].

direction, toward point F. If the irradiance is still rapidly increasing, the PV power curve will move to G on curve 3 instead of to F on curve 2. Again the MPPT will see a positive ΔP and will assume it is moving toward the MPP, continuing to perturb to point I. From points A to D to G to I the MPPT is continually moving away from the MPP, decreasing the efficiency of the P&O algorithm. This situation can occur on partly cloudy days, when MPP tracking is most difficult, owing to the frequent movement of the MPP.

There are several improvements of the P&O algorithm have been proposed, and one of the simplest entails the addition of a 'waiting' function that causes a momentary cessation of

Table 2
Summary of hill climbing and P&O algorithm [44].

Perturbation	Charge in power	Next perturbation
Positive	Positive	Positive
Positive	Negative	Negative
Negative	Positive	Negative
Negative	Negative	Positive

perturbations if the algebraic sign of the perturbation is reversed several times in a row, indicating that the MPP has been reached. This reduces the oscillation about the MPP in the steady state and improves the algorithm's efficiency under constant irradiance conditions. However, it also makes the MPPT slower to respond to changing atmospheric conditions, worsening the erratic behavior on partly cloudy days. Another modification involves measuring the array's power P_1 at array voltage V_1, perturbing the voltage and again measuring the array's power, P_2, at the new array voltage V_2, and then changing the voltage back to its previous value and re-measuring the array's power, P_1', at V_1. From the two measurements at V_1, the algorithm can determine whether the irradiance is changing. Again, as with the previous modifications, increasing the number of samples of the array's power slows the algorithm down. Also, it is possible to use the two measurements at V_1 to make an estimate of how much the irradiance has changed between sampling periods, and to use this estimate in deciding how to perturb the operating point. This, however increases the complexity of the algorithm, and also slows the operation of the MPPT [18].

From Fig. 6, it can be seen that incrementing (decrementing) the voltage increases (decreases) the power when operating on the left of the MPP and decreases (increases) the power when on the right of the MPP. Therefore, if there is an increase in power, the subsequent perturbation should be kept the same to reach the MPP and if there is a decrease in power, the perturbation should be reversed. This algorithm is summarized in Table 2.

D'Souza et al. [35], pointed out that the algorithm also works when instantaneous (instead of average) PV array voltage and current are used, as long as sampling occurs only once in each switching cycle. The process is repeated periodically until the MPP is reached. The system then oscillates about the MPP. The oscillation can be minimized by reducing the perturbation step size. However, a smaller perturbation size slows down the MPPT. A solution to this conflicting situation is to have a variable perturbation size that gets smaller towards the MPP as shown in [25,29,32,33]. In [35], fuzzy logic control is used to optimize the magnitude of the next perturbation. In [13], a two-stage algorithm is proposed that offers faster tracking in the first stage and finer tracking in the second stage. On the other hand, Tafticht and Agbossou [45], bypasses the first stage by using a nonlinear equation to estimate an initial operating point close to the MPP.

Hill climbing and P&O methods can fail under rapidly changing atmospheric conditions as illustrated in Fig. 12. Starting from an operating point A, if atmospheric conditions stay approximately constant, a perturbation ΔV in the PV voltage V will bring the operating point to B and the perturbation will be reversed due to a decrease in power. However, if the irradiance increases and shifts the power curve from P_1 to P_2 within one sampling period, the operating point will move from A to C.

This represents an increase in power and the perturbation is kept the same. Consequently, the operating point diverges from the MPP and will keep diverging if the irradiance steadily increases. To ensure that the MPP is tracked even under sudden changes in irradiance, Hsiao and Chen [46], use a three-point weight comparison P&O method that compares the actual power point to two preceding ones before a decision is made about the perturbation sign. Femia et al [33], have been optimized the sampling, while in [35], simply a high sampling rate is used. Xiao and Dunford [25], have introduced a toggling between the traditional hill climbing algorithm and a modified adaptive hill climbing mechanism to prevent deviation from the MPP.

Kasa et al. [36] estimated the PV array current from the PV array voltage, eliminating the need for a current sensor. Digital signal processor (DSP) or microcomputer control is more suitable for hill climbing and P&O even though discrete analog and digital circuitry can be used as in [21].

(iv) **Incremental conductance**

The incremental conductance (IncCond) algorithm is derived by differentiating the PV array power with respect to voltage and setting the result equal to zero [49]. This is shown in the following equation:

$$\frac{dP}{dV} = \frac{d(VI)}{dV} = I + V\frac{dI}{dV} = 0 \text{ at the MPP} \tag{2}$$

Rearranging Eq. (2) gives

$$-\frac{I}{V} = \frac{dI}{dV} \tag{3}$$

Note that the left-hand side of Eq. (3) represents the opposite of the PV array's instantaneous conductance, while the right-hand side represents its incremental conductance.

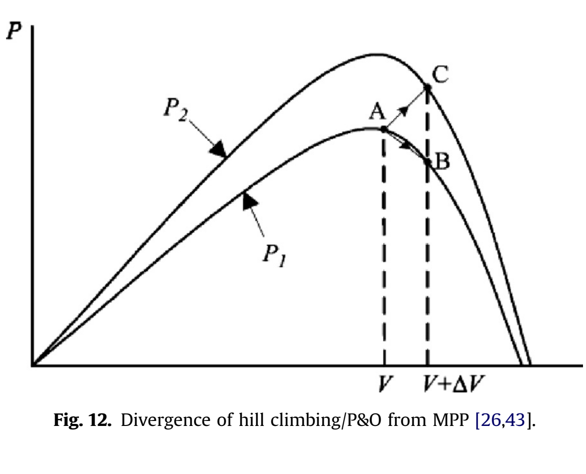


Fig. 12. Divergence of hill climbing/P&O from MPP [26,43].

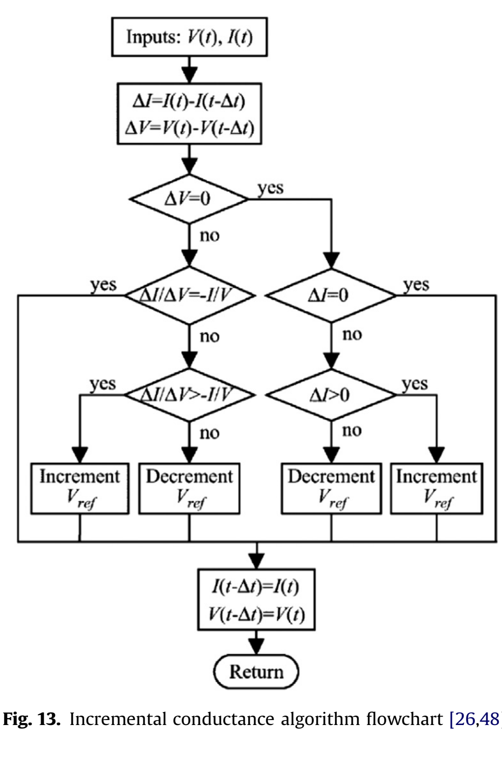


Fig. 13. Incremental conductance algorithm flowchart [26,48].

Thus, at the MPP, these two quantities must be equal in magnitude, but opposite in sign. If the operating point is off of the MPP, a set of inequalities can be derived from Eq. (3) that indicates whether the operating voltage is above or below the MPP voltage.

These relationships [47] are summarized in the following equations:

$$\frac{dI}{dV} = -\frac{I}{V}; \quad \left(\frac{dP}{dV} = 0\right), \quad \text{at MPP} \tag{4a}$$

$$\frac{dI}{dV} > -\frac{I}{V}; \quad \left(\frac{dP}{dV} > 0\right), \quad \text{left of MPP} \tag{4b}$$

$$\frac{dI}{dV} < -\frac{I}{V}; \quad \left(\frac{dP}{dV} < 0\right), \quad \text{right of MPP} \tag{4c}$$

Eq. (4a) is a repeat of Eq. (3) for convenience. Eqs. (4b) and (4c) are used to determine the direction in which a perturbation must occur to move the operating point toward the MPP, and the perturbation is repeated until Eq. (4a) is satisfied. Once the MPP is reached, the MPPT continues to operate at this point until a change in current is measured. This change in current will correlate to a change in irradiance on the array.

As the irradiance on the array increases, the MPP moves to the right with respect to the array voltage, as shown in Fig. 10. To compensate for this movement of the MPP, the MPPT must increase the array's operating voltage. The opposite is true when a decrease in irradiance is detected (via a decrease in the measured current).

From the above mentioned it is clear that, the IncCond [26,48] method is based on the fact that the slope of the PV array power curve (Fig. 10) is zero at the MPP, positive on the left of the MPP, and negative on the right.

Fig. 13 shows a flowchart for the incremental conductance algorithm [49]. The present value and the previous value of the solar array voltage and current are used to calculate the values of dI and dV. If $dV=0$ and $dI=0$, then the atmospheric conditions have not changed and the MPPT is still operating at the MPP. If $dV=0$ and $dI>0$, then the amount of sunlight has increased, raising the MPP voltage.

This requires the MPPT to increase the PV array operating voltage to track the MPP. Conversely, if $dI<0$, the amount of sunlight has decreased, lowering the MPP voltage and requiring the MPPT to decrease the PV array operating voltage. If the changes in voltage and current are not zero, the relationships in Eqs. (4b) and (4c) can be used to determine the direction in which the voltage must be changed in order to reach the MPP. If $dI/dV>I=V$, then $dP/dV>0$, and the PV array operating point is to the left of the MPP on the P–V curve. Thus, the PV array voltage must be increased to reach the MPP. Similarly, if $dI/dV<I=V$, then $dP/dV<0$ and the PV array operating point lies to the right of the MPP on the P–V curve, meaning that the voltage must be reduced to reach the MPP. Herein lies a primary advantage of incremental conductance over the perturb-and-observe algorithm: incremental conductance can actually calculate the direction in which to perturb the array's operating point to reach the MPP, and can determine when it has actually reached the MPP. Thus, under rapidly changing conditions, it should not track in the wrong direction, as P&O can, and it should not oscillate about the MPP once it reaches it.

The increment size determines how fast the MPP is tracked. Fast tracking can be achieved with bigger increments but the system might not operate exactly at the MPP and oscillate about it instead; so there is a tradeoff.

Kobayashi et al. [49] proposed a method that brings the operating point of the PV array close to the MPP in a first stage and then uses IncCond to exactly track the MPP in a second stage. Through proper control of the power converter, the initial operating point is set to match a load resistance proportional to the ratio of the open-circuit voltage (V_{OC}) to the short-circuit current (I_{SC}) of the PV array. This two-stage alternative also ensures that the real MPP is tracked in case of multiple local maxima.

Measurements of the instantaneous PV array voltage and current require two sensors. The IncCond method lends itself well to DSP and microcontroller control, which can easily keep track of previous values of voltage and current and make all the decisions as per Fig. 13.

(v) **Constant voltage and current**

The basis for the constant voltage (C_V) algorithm is the observation from I–V curves like those in Fig. 1 that the ratio of the array's maximum power voltage, V_{MPP}, to its open-circuit voltage, V_{OC}, is approximately constant; in other words:

$$\frac{V_{MPP}}{V_{OC}} \cong K < 1 \tag{5}$$

The constant voltage algorithm can be implemented using the flowchart shown in Fig. 14. The solar array is temporarily isolated from the MPPT, and a V_{OC} measurement is taken. Next, the MPPT calculates the correct operating point using Eq. (5) and the preset value of K, and adjusts the array's voltage until the calculated V_{MPP} is reached. This operation is repeated periodically to track the position of the MPP.

Although this method is extremely simple, it is difficult to choose the optimal value of the constant K. The literature reports success with K values ranging from 73% to 80% [10–12]. Fig. 15 shows the actual K values required for a given PV array over a temperature range of 0–60 °C and irradiance levels from 200 to 1000 W/m^2.

These curves were calculated using the I–V relationship for a PV cell given in the following equations:

$$I = I_L - I_{OS}\left[\exp\frac{q}{Ak_BT}(V+IR) - 1\right] \tag{6}$$

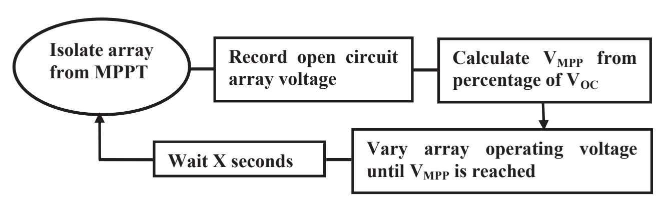


Fig. 14. Constant voltage algorithm flowchart [18].

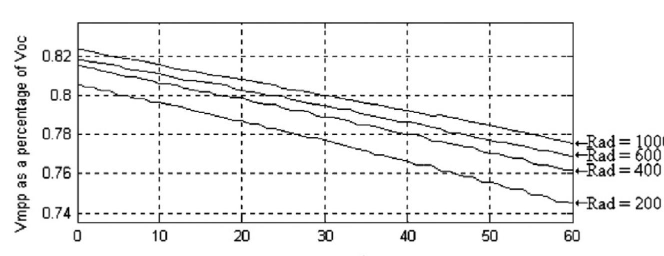


Fig. 15. V_{MPP} as a percentage of V_{OC} as functions of temperature and irradiance [18].

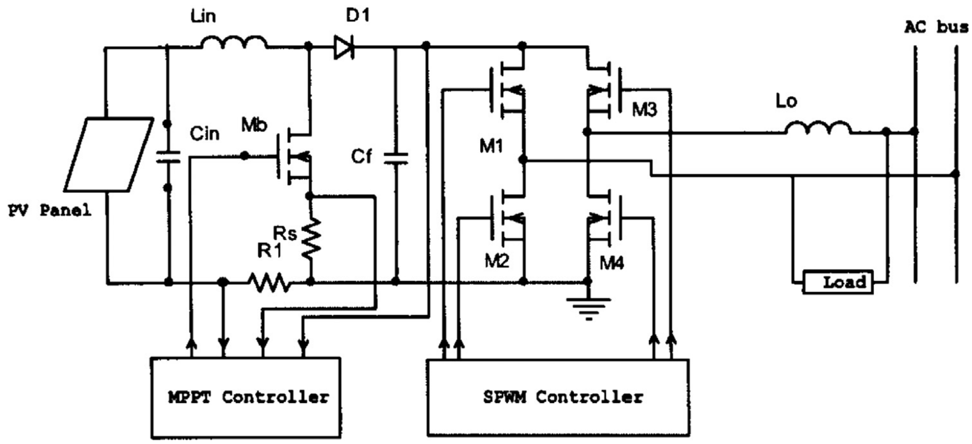


Fig. 16. Power circuit of proposed converter system [58].

$$I_{OS} = I_{OR}\left(\frac{T}{T_R}\right)\exp\left[\frac{qE_G}{Ak_B}\left(\frac{1}{T_R}-\frac{1}{T}\right)\right] \tag{7}$$

$$I_L = \left(\frac{G}{1000}\right)\left[I_{SC} + K_{T,I}(T-T_R)\right] \tag{8}$$

Eq. (6) is the Shockley equation for an illuminated pn junction. A is the diode ideality factor, q is the charge on an electron, and R is the PV array's series resistance. (The shunt resistance has been assumed large enough to be accurately approximated as infinite.) Eq. (7) accounts for the temperature dependency of the reverse saturation current I_{OS}. I_{OS} is a function of the reference reverse saturation current I_{OR} at the standard test condition reference temperature T_R (25 °C), E_G, the bandgap of the semiconductor used, the measured cell temperature T (°C), Boltzmann's constant k_B, and the charge on an electron q. Eq. (8) gives the light generated current I_L as a function of irradiance G (W/m^2), the array's short-circuit current at standard test conditions I_{SC}, the temperature coefficient for current of the array $K_{T,I}$ (A/°C), (which is typically very small), and the array temperature T (°C). Fig. 15 indicates that the ratio K is not constant, but in fact depends on temperature and irradiance and varies by as much as 8% (absolute) over the entire range of conditions.

Constant voltage control can be easily implemented with analog hardware. However, its MPPT tracking efficiency is low relative to those of other algorithms. Reasons for this include the aforementioned error in the value of K, and the fact that measuring the open-circuit voltage requires a momentary interruption of PV power. It is possible to dynamically adjust the value of K, but that requires a search algorithm and essentially ends up being the same as P&O [18].

In [50], it is possible to use a constant current MPPT algorithm that approximates the MPP current as a constant percentage of the short-circuit current. To implement this algorithm, a switch is placed across the input terminals of the converter and switched on momentarily. The short-circuit current is measured and the MPP current is calculated, and the PV array output current is then adjusted by the MPPT until the calculated MPP current is reached. This operation is repeated periodically. However, constant voltage control is normally favored because of the relative ease of measuring voltages, and because open-circuiting the array is simple to accomplish, but it is not practically possible to short-circuit the array and still make a current measurement.

(vi) **Fractional open-circuit voltage**

The near linear relationship between V_{MPP} and V_{OC} of the PV array, under varying irradiance and temperature levels, has given rise to the fractional V_{OC} method [51–55].

$$V_{MPP} \approx k_1 V_{OC} \tag{9}$$

where k_1 is a constant of proportionality. Since k_1 is dependent on the characteristics of the PV array being used, it usually has to be computed beforehand by empirically determining V_{MPP} and V_{OC} for the specific PV array at different irradiance and temperature levels. The factor k_1 has been reported to be between 0.71 and 0.78. Once k_1 is known, V_{MPP} can be computed using Eq. (9) taking into consideration measuring of V_{OC} periodically by momentarily shutting down the power converter. But, this incurs some disadvantages, including temporary loss of power. Kobayashi et al. [49] mentioned that the voltage generated by pn-junction diodes is approximately 75% of V_{OC}. This eliminates the need for measuring V_{OC} and computing V_{MPP}. Once V_{MPP} has been approximated, a closed-loop control on the array power converter can be used to asymptotically reach this desired voltage.

Since Eq. (29) is only an approximation, the PV array technically never operates at the MPP. Depending on the application of the PV system, this can sometimes be adequate. Even if fractional V_{OC} is not a true MPPT technique, it is very easy and cheap to implement as it does not necessarily require DSP or microcontroller control.

(vii) **Modified open-circuit voltage method**

In this method, the PV array is not temporarily isolated from MPPT, the open circuit voltage (V_{OC}) is calculated for different values of insolation and temperature [56] by making use of the following equations:

$$C_{TV} = \left(\frac{V_{OCT}}{V_{OC}}\right) = 1 + \left(\frac{k_v}{V_{OC}}\right)(T_x - T_c) \tag{10}$$

where k_v is the temperature coefficient of V_{OC}. The value of k_v taken is −0.16 V/°C

$$C_{SV} = 1 + \beta_T \alpha_s (S_x - S_c) \tag{11}$$

where $\alpha_s = (dT_c/S_x - S_c)$, dT_C is temperature change due to change in irradiation. The values of β_T and α_s taken are 0.0042 and 0.0061 respectively. So overall effect of temperature and insolation on open circuit voltage is

$$V_{OC(TG)} = C_{TV} C_{SV} V_{OC} \tag{12}$$

There is no shutdown of power converter periodically, hence will not incur any temporary loss of power.

(viii) **Pilot cell**

In the pilot cell MPPT algorithm, the constant voltage or current method is used, but the open-circuit voltage or short-circuit current measurements are made on a small solar cell, called a pilot cell, that has the same characteristics as the cells in the larger solar array [50]. The pilot cell measurements can be used by the MPPT to operate the main solar array at its MPP, eliminating the loss of PV power during the V_{OC} or I_{SC} measurement [57].

However, the problem of a lack of a constant K value is still present. Also, this method has a logistical drawback in that the solar cell parameters of the pilot cell must be carefully matched to those of the PV array it represents. Thus, each pilot cell/solar array pair must be calibrated, increasing the energy cost of the system. These pilot cells must be carefully chosen to closely represent the characteristics of the PV array.

(ix) **Fractional short-circuit current**

Several authors [52,55,57] pointed out that the fractional I_{SC} results from the fact that, under varying atmospheric conditions, I_{MPP} is approximately linearly related to the I_{SC} of the PV array.

$$I_{MPP} \approx k_2 I_{SC} \tag{13}$$

where k_2 is a proportionality constant. Just like in the fractional V_{OC} technique, k_2 has to be determined according to the PV array in use. The constant k_2 is generally found to be between 0.78 and 0.92.

Measuring I_{SC} during operation is problematic. An additional switch usually has to be added to the power converter to periodically short the PV array so that *ISC* can be measured using a current sensor. This increases the number of components and cost. Bekker and Beukes [55] mentioned that, proper MPPT can be guarantee in the presence of multiple local maxima by periodically sweeps the PV array voltage from open-circuit to short-circuit to update k_2. Most of the PV systems using fractional I_{SC} in the literature use a DSP.

Yuvarajan and Xu [58] proposed a MPP tracking by measuring the short circuit current I_{SC} and adjusting the actual load current to be equal to a desired fraction of I_{SC}. The power circuit of the PV converter is shown in Fig. 16. The scheme is used to supply 60 Hz ac power to the ac mains and to some local loads. The dc voltage from the PV panel is stepped up by the boost converter made up of the inductor L_{in} switch M_b, and diode D_1. The output from the boost converter will charge the capacitor C_f. A separate feedback loop is used to regulate the output voltage of the boost converter by adjusting the duty cycle of the gate pulses. A reasonably regulated dc voltage is thus fed to the inverter. Switches M_1 to M_4 form the bridge inverter for converting the output voltage of the boost converter and feeding it into a 60 Hz ac bus. The inductor L_o is used to remove the high-frequency ripple from the output voltage.

The current I_{SC} is measured by shorting the panel by turning on M_b periodically. This is done by applying pulses with a width relatively larger than those used for boost action. A divide-by-N counter is used obtain these pulses from the boost pulses. The voltage across the sensing resistor R_S represents the short-circuit current. The current pulses sensed during the extended intervals have transient peaks in addition to steady state portion. They are further processed using a sample- and hold (S/H) circuit. The output of the S/H circuit becomes the short circuit current I_{SC}. It is to be noted that the presence of the capacitor C_{in} across the PV panel will not affect the steady state value of the short-circuit current measured by the circuit. The load current supplied by the PV panel is sensed by using a small series resistor R_1. A low-pass filter is used to remove the high-frequency ripple from the sensed output. The duty cycle of the pulses applied to M_b is adjusted until the actual load current is equal to the desired fraction of I_{SC}. This will be implemented using a simple current feedback loop. Since the rate of variation of light intensity is low, it is possible to achieve a satisfactory response by using a simple proportional controller.

The output of the bridge inverter is supplied to the grid. In order to keep the duty cycle of M_b within practical limits, the modulation index of the inverter can be varied. If the output voltage of the PV panels is low, a high frequency transformer can be inserted between the inverter bridge and the filter inductor L_o.

(x) **Modified short-circuit current method**

The short circuit current varies due to temperature and insolation both. The combined effect is taken into account to calculate short circuit current for different conditions of temperature and insolation [56] by using the following equations.

The variation of short circuit current with temperature is [59],

$$C_{TI} = \frac{I_{SCT}}{I_{SC}} = 1 + k_I(T_x - T_c) \tag{14}$$

where value of k_I is 0.0006 A/°C.

The variation of short circuit current with insolation (S) is [59],

$$C_{SI} = \frac{I_{SCG}}{I_{SC}} = \frac{S_X}{S_C} \tag{15}$$

where S_X and S_C are insolations at variable and reference conditions.

The variation of short circuit current with temperature and insolation is [59],

$$I_{SC(TG)} = C_{TI} C_{SI} I_{SC} \tag{16}$$

There is no shutdown of power converter periodically, hence will not incur any temporary loss of power.

(xi) **Parasitic capacitance/dc-link capacitor droop control**

The parasitic capacitance algorithm is similar to incremental conductance, except that the effect of the solar cells' parasitic junction capacitance C_P, which models charge storage in the p–n junctions of the solar cells, is included. By adding this capacitance to the lighted diode equation, Eq. (6), and representing the capacitance using $i(t)=CdV/dt$, the following equation is obtained [60].

$$I = I_L - I_O\left[\exp\left(\frac{V_p + R_S I}{a}\right) - 1\right] + C_P\frac{dv_p}{dt} = F(v_p) + C_P\frac{dv_p}{dt} \tag{17}$$

On the far right of Eq. (17), the equation is rewritten to show the two components of I, a function of voltage $F(v_p)$ and the current in the parasitic capacitance. Using this notation, the incremental conductance of the array g_P can be defined as $dF(v_p)/dv_p$ and the instantaneous conductance of the array, g_L can be defined as $-F(v_p)/v_p$. The MPP is located at the point where $dP/dv_p = 0$. Multiplying Eq. (17) by the array voltage v_p to obtain array power and differentiating the result, the equation for the array power at the MPP is

obtained [60]:

$$\frac{dF(v_p)}{dv_p} + C_P\left(\frac{\dot{V}}{V} + \frac{\ddot{V}}{\dot{V}}\right) + \frac{F(v_p)}{v_p} = 0 \tag{18}$$

The three terms in Eq. (18) represent the instantaneous conductance, the incremental conductance, and the induced ripple from the parasitic capacitance. The first and second derivatives of the array voltage take into account the ac ripple components generated by the converter. The reader will note that if C_P is equal to zero, this equation simplifies to that used for the incremental conductance algorithm. Since the parasitic capacitance is modeled as a capacitor connected in parallel with the individual solar cells, connecting the cells in parallel will increase the effective capacitance seen by the MPPT. From this, the difference in MPPT efficiency between the parasitic capacitance and incremental conductance algorithms should be at a maximum in a high-power solar array with many parallel modules.

The array conductance is easily calculated, since it is just the ratio of the instantaneous array current to the instantaneous array voltage. Obtaining the array differential conductance is more difficult, but it can be done [60] using the equation

$$g_p = \frac{P_{GP}}{V_O^2} = \frac{\frac{1}{2}\sum_{n=1}^{\infty}[a_n^i a_n^v + b_n^i b_n^v]}{\frac{1}{2}\sum_{n=1}^{\infty}[(a_n^v)^2 + (b_n^v)^2]} \tag{19}$$

where P_{GP} is the average ripple power, V_O is the magnitude of the voltage ripple, and a_n^i, a_n^v, b_n^i, b_n^v are the coefficients of the Fourier series of the PV array voltage and current ripples.

The values of P_{GP} and V_O^2 may be obtained from a circuit configuration like that seen in Fig. 17. The inputs to the circuit are the measured array current and voltage. The high-pass filters remove the dc component of VPV.

The two multipliers generate the ac V_O^2 and ac P_{GP}, which are then filtered by the low-pass filters, leaving behind the dc components of V_O^2 and P_{GP}. From Eq. (19), the ratio of these two values is equal to the array conductance, which can then be used in conjunction with Eq. (20) until the array differential conductance and the array conductance are equal [18].

dc-Link capacitor droop control [61–63] is an MPPT technique that is specifically designed to work with a PV system that is connected in parallel with an ac system line as shown in Fig. 18. The duty ratio of an ideal boost converter is given by

$$d = 1 - \frac{V}{V_{link}} \tag{20}$$

where V is the voltage across the PV array and V_{link} is the voltage across the dc link. If V_{link} is kept constant, increasing the

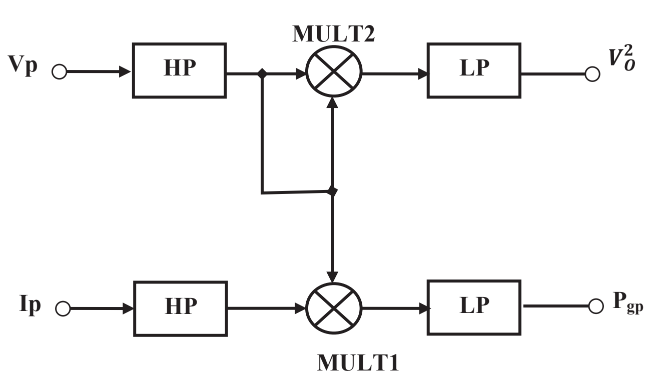


Fig. 17. Circuitry used to implement the parasitic capacitance method [60].

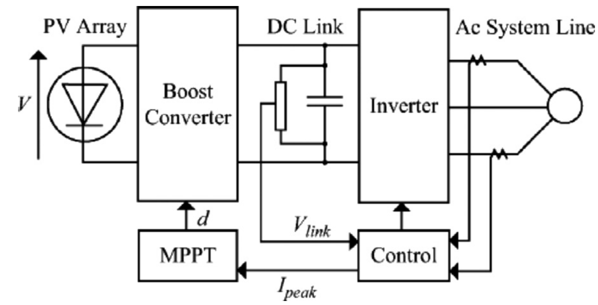


Fig. 18. Topology for dc-link capacitor droop control as shown in [62].

current going in the inverter increases the power coming out of the boost converter and consequently increases the power coming out of the PV array. While the current is increasing, the voltage V_{link} can be kept constant as long as the power required by the inverter does not exceed the maximum power available from the PV array. If that is not the case, V_{link} starts drooping. Right before that point, the current control command I_{peak} of the inverter is at its maximum and the PV array operates at the MPP. The ac system line current is fed back to prevent V_{link} from drooping and d is optimized to bring I_{peak} to its maximum, thus achieving MPPT.

dc-Link capacitor droop control does not require the computation of the PV array power, but according to [62], its response deteriorates when compared to a method that detects the power directly; this is because its response directly depends on the response of the dc-voltage control loop of the inverter. This control scheme can be easily implemented with analog operational amplifiers and decision-making logic units.

The dc link capacitor (C_{dc}) reduces the voltage ripple in the input to the dc–ac inverter and also provides a hold-up time during which the insolation swings quickly between high and low. However the C_{dc} should not be so high as not to implement the MPPT algorithm. The dc link capacitor C_{dc} is calculated as a function of the desired hold-up time [64]:

$$C_{dc} \approx 2\frac{\text{Rated power output} \times \text{hold}-\text{up time}}{(V_{d,\text{nominal}}^2 - V_{d,\min}^2)\eta} \tag{21}$$

where $V_{d,min}$ is chosen to be in the range of 60–75% of the nominal input voltage ($V_{d,\text{nominal}}$) and η is the energy efficiency of the power supply. The output L filter is used to filter out undesired switching frequency components from the output current spectrum [65].

$$L = \frac{V_g}{2\sqrt{6} f_s i_{ripple-peak}} \tag{22}$$

where V_g is the grid rms phase voltage, and f_s is inverter switching frequency. As for a large scale PV grid-connected system, the LCL filter design is the optimum choice [65].

(xii) ***dP/dV* or *dP/dI* feedback control**

With DSP and microcontroller being able to handle complex computations, an obvious way of performing MPPT is to compute the slope differential power to voltage or differential power to voltage current (dP/dV or dP/dI) of the PV power curve (Fig. 6) and feed it back to the power converter with some control to drive it to zero. This is exactly what is done in [66,67].

Many of MPPT techniques calculate the reference voltage according to the power–voltage curves in order to implement the MPPT strategy. The relation of dP/dV versus V is nonlinear, thus, the various methods of MPPT according to the relation of dP/dV–V have various deficient such as the

question of complication, non-smoothing, and instability. However, the relation between the dP/dV and output current of the PV array is proved to be almost linear near the maximum power point (MPP) region [68]. The new standard of IEEE 929-2000 limits the current THD of 5% with a power factor close enough to unity [69].

The way the slope is computed differs from paper to paper. In [66], dP/dV is computed and its sign is stored for the past few cycles. Based on these signs, the duty ratio of the power converter is either incremented or decremented to reach the MPP. A dynamic step size is used to improve the transient response of the system. In [67,70], sampling and data conversion are used with subsequent digital division of power and voltage to approximate dP/dV. In [70], dP/dI is then integrated together with an adaptive gain to improve the transient response. In [67], the PV array voltage is periodically incremented or decremented and $\Delta P/\Delta V$ is compared to a marginal error until the MPP is reached.

In order to meet the requirements of the IEEE 929-2000 standard, a new maximum power point tracking applying the relation between dP/dV and I of a photovoltaic array combined with space vector pulse width modulation (SVPWM) current-controlled scheme has been proposed and verified through an experimental 3-phase grid-connected PV system [71]. To improve the dynamic response for over-current protection, a dual-timer scheme for PWM carrier and ADC sampling has been developed to greatly decrease the control delay.

Since at MPP the derivative power to voltage is zero ($dP/dV=0$), [71], the developed MPPT algorithm is based on the characteristic of the PV array's deferential power to the voltage which is shown in Fig. 19.

The first step is to set up a working voltage whose value is about 0.8 times of the PV array open voltage. Then measuring the instantaneous voltage and current of the PV

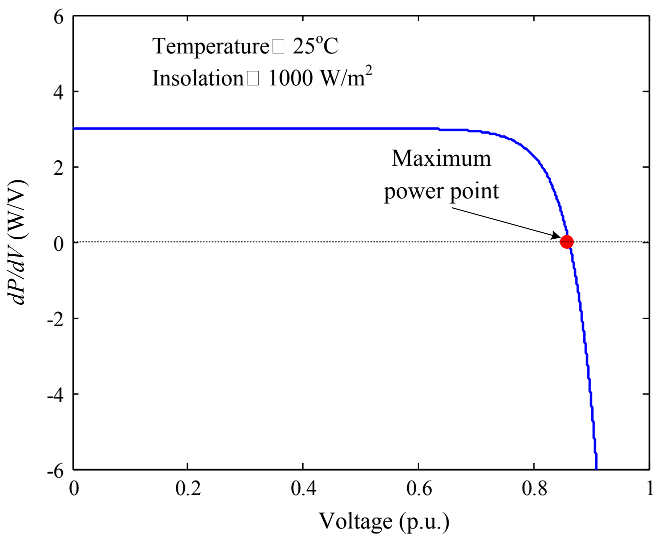


Fig. 19. The dP/dV–V curve of PV array [71].

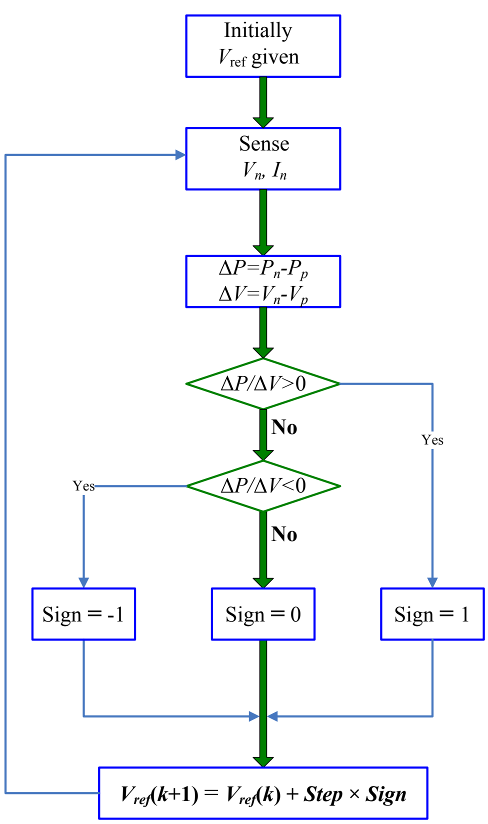


Fig. 20. The flowchart of developed MPPT algorithm [71].

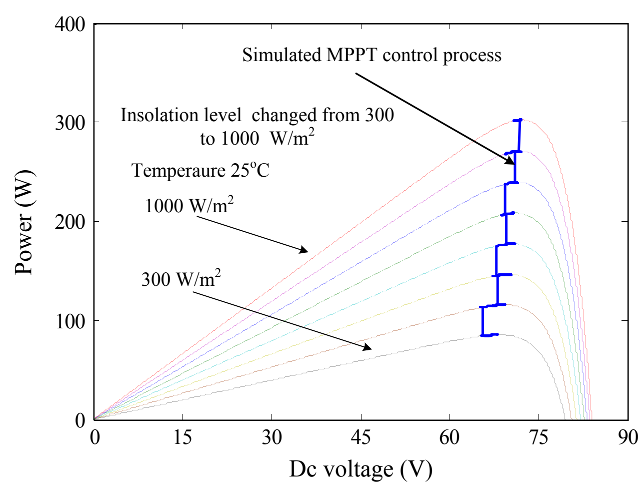


Fig. 21. The simulated P–V curves by the MPPT algorithm [71].

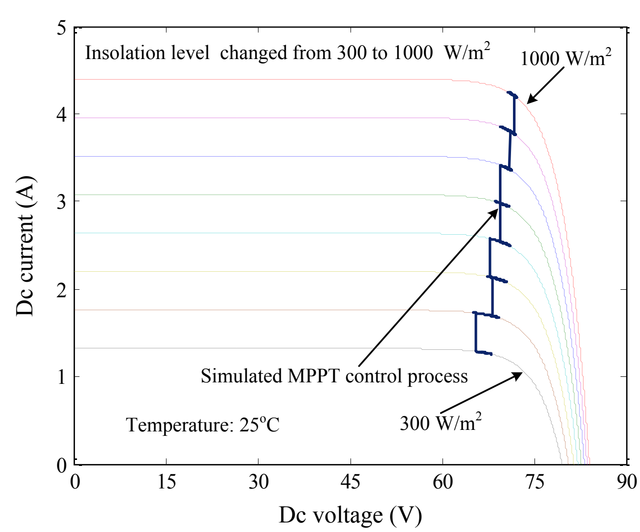


Fig. 22. The simulated I–V curves by the MPPT algorithm [71].

array, using the saved previous voltage and current (V_p and I_p) to calculate the differential values of ΔP and ΔV. The $\Delta P/\Delta V$ is calculated by using Newton–Raphson algorithm which is written in C language fixed-point algorithm for a TMS320F2812 digital control process. Then judgment: When the $\Delta P/\Delta V$ is more than 0, the *sign* value is set to 1; When the $\Delta P/\Delta V$ is less than 0, the *sign* value is set to −1; Or else the *sign* value is set to 0. The reference voltage of the MPP of the PV array is given as follows:

$$V_{ref}(k+1) = V_{ref}(k) + Step \times Sign \tag{23}$$

where the variable *Step* is assigned to 0.1 mV and the frequency of sampling voltage and current of PV array is 0.1 ms. The developed MPPT algorithm can provide the reference voltage of MPP for PV array quickly and smoothly, which reduces the losses of the PV array by using P&O method and is not complicated comparing with the IncCond method. The proposed MPPT control flow chart is shown in Fig. 20.

The sampling rate for PV dc voltage and dc current is 100 μs in order to adapt the MPPT algorithm. Figs. 21 and 22 show the simulated PV power versus voltage and current versus voltage curves, respectively, by the proposed MPPT algorithm under the different levels of insolation. It can be noticed that the performances of both the MPPT and the dc controller $PI_{dc}(s)$ are very good. The dc link voltage is controlled to track the maximum power point's voltage-reference.

(xiii) **Fuzzy logic controller (FLC)**

Several microcontrollers have made using FLC for MPPT [72–77]. Veerachary et al. [76] mentioned that, the FLC have the advantages of working with imprecise inputs, it does not need an accurate mathematical model and it can handle nonlinearity as well. FLC constitutes four parts, which include fuzzification, inference, rule base and defuzzification as shown in Fig. 23 [78,79].

The inputs to a MPPT fuzzy logic controller are usually an error E and a change in error ΔE. The user has the flexibility of choosing how to compute E and ΔE. Since dP/dV vanishes at the MPP, [77] uses the approximation:

$$E(n) = \frac{P(n)-P(n-1)}{V(n)-V(n-1)} \tag{24}$$

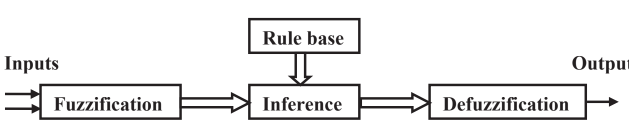


Fig. 23. Block diagram of fuzzy logic controller.

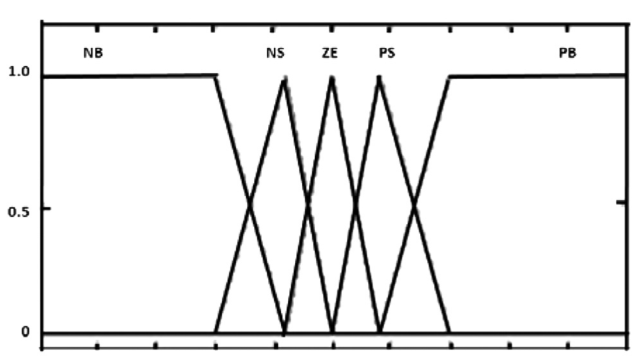


Fig. 24. Membership function of $E(n)$ and $CE(n)$.

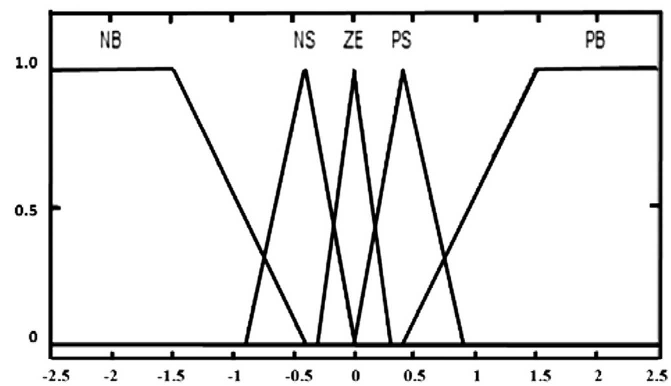


Fig. 25. Membership function of $V(n)$.

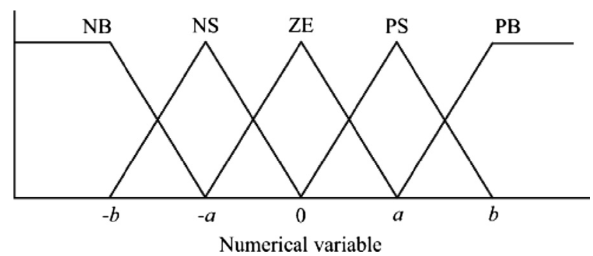


Fig. 26. Membership function for inputs and output of fuzzy logic controller.

Table 3
Fuzzy rule base table.

E	ΔE				
	NB	NS	ZE	PS	PB
NB	ZE	ZE	NB	NB	NB
NS	ZE	ZE	NS	NS	NS
ZE	NS	ZE	ZE	ZE	PS
PS	PS	PS	PS	ZE	ZE
PB	PB	PB	PB	ZE	ZE

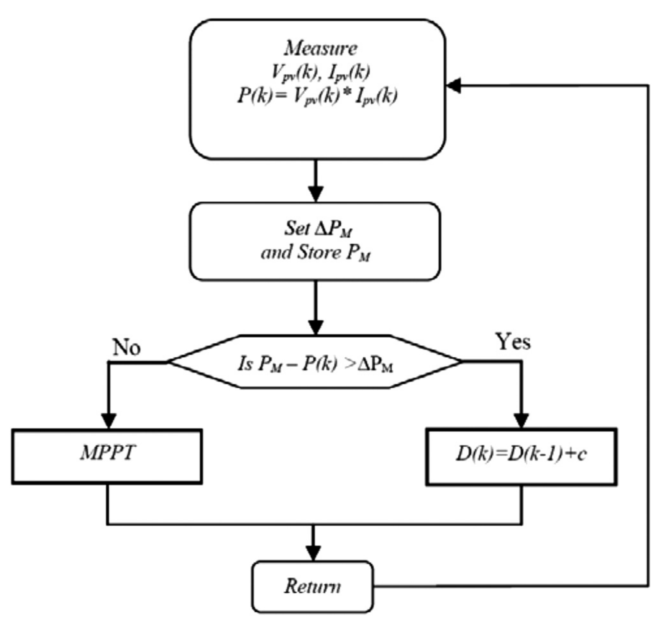


Fig. 27. A modified fuzzy-logic controller for maximum power point tracking [81].

and

$$\Delta E(n) = E(n) - E(n-1) \tag{25}$$

During fuzzification, the numerical input variables are converted into linguistic variables based on the membership functions as shown in Figs. 24–26 [78]. Five fuzzy levels are used for all the inputs and outputs variables: negative big (NB), negative small (NS), zero (ZE), positive small (PS), and positive big (PB).

Table 4
Fuzzy logic rules [81].

ΔP	ΔI				
	NB	**NS**	**PS**	**PB**	ΔP_M
NB	PM	PM	NM	NM	PS
NS	PS	PS	NS	NS	
PS	NS	NS	PS	PS	
NB	NM	NM	PM	PM	
NB	PB	PB	PB	PB	PB
NS	PB	PB	PB	PB	
PS	PB	PB	PB	PB	
PB	PB	PB	PB	PB	

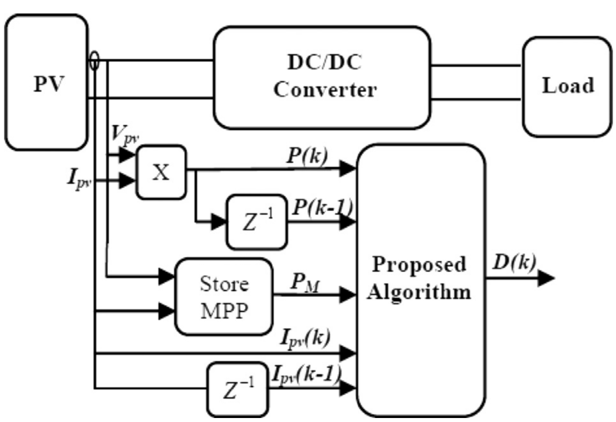


Fig. 28. PV array system block diagram and the proposed MPPT controller [81].

In this case, five fuzzy levels are used: NB, NS, ZE, PS, and PB. For more accuracy, seven fuzzy levels are used as in [74,75]. In Fig. 26, symbols a and b are based on the range of values of the numerical variable. The membership function is sometimes made less symmetric to give more importance to specific fuzzy levels as in [73,76,77].

The effective way of performing the IncCond technique is to use the instantaneous conductance and the incremental conductance to generate an error signal as suggested by Harada and Zhao [80]

$$e = \frac{I}{V} + \frac{dI}{dV} \tag{26}$$

Once E and ΔE are calculated and converted to the linguistic variables, the fuzzy logic controller output, which is typically a change in duty ratio ΔD of the power converter, can be looked up in a rule base table such as Table 3 [72].

Alajmi et al. [81] proposed a modification to the fuzzy logic based MPPT algorithm, using scanning and storing procedure to quickly locate the global maximum power point. A mathematical model has been proposed to represent the behavior of the PV characteristic under partial shadowing conditions. Fig. 27 shows the flow chart of modified fuzzy-logic controller for MPPT, where V_{pv} are I_{pv} are the PV output voltage and current respectively, D is the duty cycle, P_m is the global maximum power point, and ΔP_m is a constant that identifies the allowable difference between the global maximum and the operating power point. The inputs to the fuzzy logic controller (FLC) are

$$\Delta P = P(k) - P(k-1) \tag{27}$$

$$\Delta I = I(k) - I(k-1) \tag{28}$$

$$\Delta P_M = P_m(k) - P(k) \tag{29}$$

and the output equation is

$$\Delta D = D(k) - D(k-1) \tag{30}$$

where ΔP and ΔI are the PV array output power and current change respectively, ΔP_M is the difference between the stored global maximum power (P_m) and the current power, and ΔD is the boost converter duty cycle change. To ensure that the PV global maximum power is stored during the scanning procedure, fast initial tracking speed was used. The variable inputs ΔP

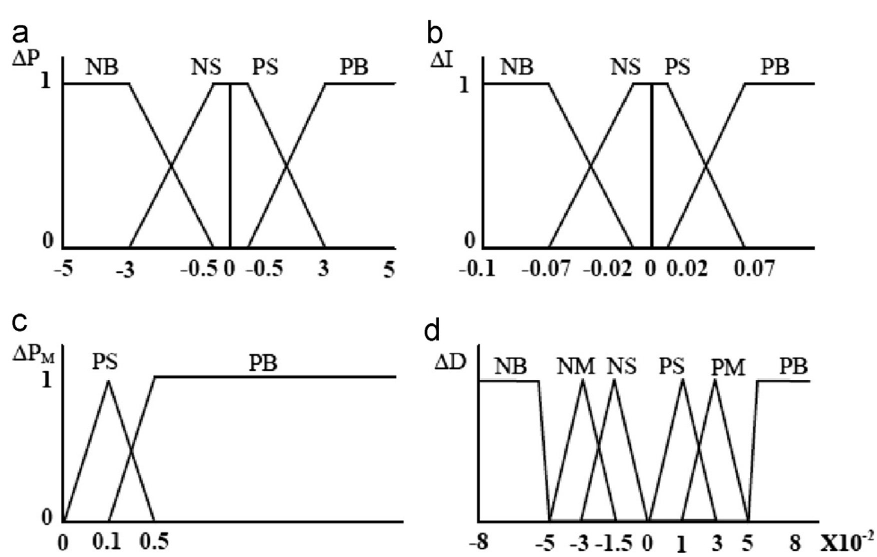


Fig. 29. Membership functions: (a) input ΔP, (b) input ΔI, (c) input ΔP_M and (d) output ΔD [81].

and ΔI were divided into four fuzzy subsets: PB, PS, NB and NS. The variable input ΔP_M was divided into two fuzzy subset: PB and PS. The output variable ΔD is divided into six fuzzy subsets: PB, Positive Medium (PM), PS, NB, Negative Medium (NM), and NS. Therefore the fuzzy algorithm requires 32 fuzzy control rules; these rules were based on the regulation of a hill climbing algorithm along with the reference power. The fuzzy rules are shown in Table 4.

During initial conditions or varying weather conditions, the initial tracking speed should be fast enough to make a wide range power scan and store the maximum available power. Also, it should be mentioned that, when the operating point reaches the global maximum, tracking speed decreases to minimize any oscillation around the global maximum point. Fig. 28 shows the PV system block diagram, along with the proposed controller.

After simulating the PV system and studying the behavior of the controller inputs and output, the shapes and fuzzy subset partitions of the membership function in both of inputs and output are shown in Fig. 29. The proposed MPPT proved to be able to reach the global maximum power point under any partial shading conditions.

FLC exhibits a better behavior than P&O method, which provides faster tracking of MPP and it presents smoother signal with less fluctuation in steady-state. It achieves very fast transient response and reduces the oscillations around MPP in steady state.

(xiv) **Load current or load voltage maximization**

As mentioned above the MPPT techniques are used to maximize the PV array output power. When the PV array is connected to a power converter, maximizing the PV array power also maximizes the output power at the load of the converter. Conversely, maximizing the output power of the converter should maximize the PV array power [82,83], assuming a lossless converter.

Shmilovitz [83] pointed out that most loads can be of voltage source type, current-source type, resistive type, or a combination of these, as shown in Fig. 30. From this figure, it is clear that for a voltage-source type load, the load current i_{out} should be maximized to reach the maximum output power PM. For a current-source type load, the load voltage v_{out} should be maximized.

For the other load types, either i_{out} or v_{out} can be used. This is also true for nonlinear load types as long as they do not exhibit negative impedance characteristics [83]. Therefore, for almost all loads of interest, it is adequate to maximize either the load current or the load voltage to maximize the load power. Hence, only one sensor is needed.

(xv) **Neural network**

Along with fuzzy logic controllers there is another technique of implementing MPPT-neural networks [84–87], which are also well adapted for microcontrollers. Neural networks commonly have three layers: input, hidden, and output layers as shown in Fig. 31. The numbers of nodes in each layer varies and are user-dependent. The input variables could be PV array parameters like V_{OC} and I_{SC}, atmospheric data like irradiance and temperature, or any combination of these. The output is usually one or several reference signal (s) like a duty cycle signal used to drive the power converter to operate at or close to the MPP.

How close the operating point gets to the MPP depends on the algorithms used by the hidden layer and how well the neural network has been trained. The links between the nodes are all weighted. The link between nodes i and j is labeled as having a weight of w_{ij} in Fig. 31 [44]. To accurately identify the MPP, the w_{ij}'s have to be carefully determined through a training process, whereby the PV array is tested over months or years and the patterns between the input (s) and output(s) of the neural network are recorded.

Since most PV arrays have different characteristics, a neural network has to be specifically trained for the PV array with which it will be used. The characteristics of a PV array also change with time, implying that the neural network has to be periodically trained to guarantee accurate MPPT [44].

(xvi) **Implementation**

A typical operation of MPPT is demonstrated in the block diagram of Fig. 32, where the controller senses and assesses the output power of the photovoltaic array and adjusts the power interface to follow the optimal operating condition. The power conditioner can be either a dc/dc converter or a dc/ac inverter. The load can be typical dc and/or ac electrical load. In grid-tied (or utility-connected) systems, the load includes the electrical utility grid [88].

Chen et al. [89] and Wanzeller et al. [90] presented topologies by regulating the PV current to follow the current of MPP. The control block diagram is illustrated in Fig. 33.

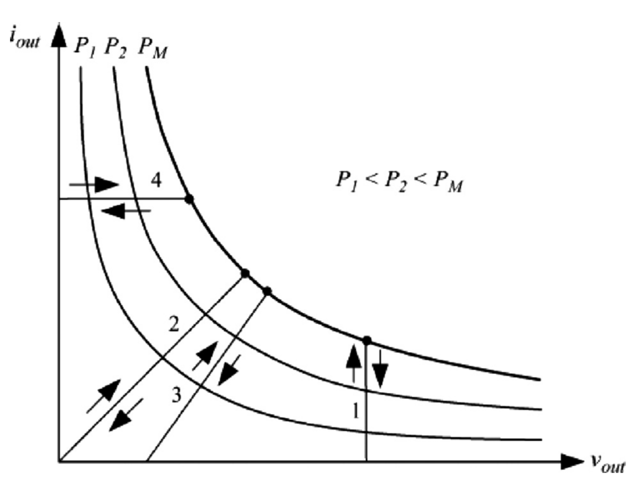


Fig. 30. Different load types. (1) Voltage source, (2) resistive, (3) resistive and voltage source, (4) current source [83].

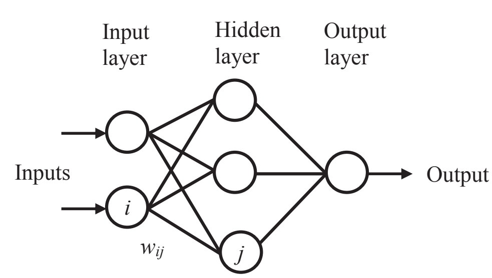


Fig. 31. Example of neural network [44].

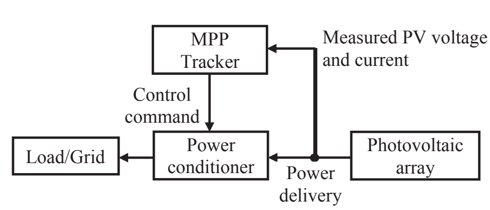


Fig. 32. Block diagram of the topology of maximum power point tracking in a photovoltaic power system.

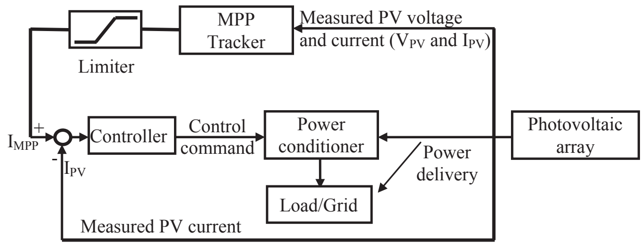


Fig. 33. Block diagram of MPPT with a control loop for regulating PV current.

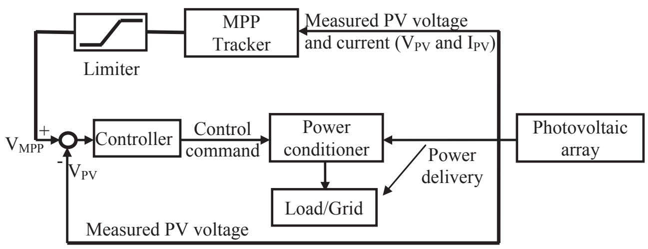


Fig. 34. Block diagram of MPPT with a control loop for regulating PV voltage.

Fig. 34 demonstrates the control scheme for MPPT by regulating the photovoltaic voltage. A comparison of PV current regulation and voltage regulation is presented in [91,92]. However, the majority of work [8,92–95] shows that the PV voltage regulation is preferable because of the following advantages:

(i) a good-quality measurement of the voltage signal is cheaper and easier than that of current detection;
(ii) the voltage of MPP is within a certain range, about 70–82% of the open-circuit voltage;
(iii) the changing insolation slightly affects the voltage of MPP;
(iv) the cell temperature is the major factor that significantly shifts the voltage of MPP; however, it has slow dynamics and is always within a certain range.

The ease of implementation is an important factor in deciding which MPPT technique to use. However, this greatly depends on the end-users' knowledge. Some might be more familiar with analog circuitry, in which case, fractional I_{SC} or V_{OC}, ripple correlation control (RCC), and load current or voltage maximization are good options. [When a PV array is connected to a power converter, the switching action of the power converter imposes voltage and current ripple on the PV array. As a consequence, the PV array power is also subject to ripple. Ripple correlation control (RCC) makes use of ripple to perform MPPT. RCC correlates the time derivative of the time-varying PV array power with the time derivative of the time-varying PV array current or voltage to drive the power gradient to zero, thus reaching the MPP.] [44].

Others might be willing to work with digital circuitry, even if that may require the use of software and programming. Then, their selection should include hill climbing/P&O, IncCond, fuzzy logic control and dP/dV or dP/dI feedback control. Furthermore, a few of the MPPT techniques only apply to specific topologies. For example, the dc-link capacitor droop control works with the system showed in Fig. 18 and the one-cycle control MPPT (OCC MPPT) works with a single-stage inverter.

(xvii) **Other MPPT techniques**

Current sweep: This method uses a sweep waveform for the PV array current such that the *I–V* characteristic of the PV array is obtained and updated at fixed time intervals. The *VMPP* can then be computed from the characteristic curve at the same intervals.

One-cycle control MPPT (*OCC MPPT*): Works with a single-stage inverter. Based on the voltage of the PV array, OCC is used to adjust the output current of the single-stage inverter such that MPPT is attained. The control circuit consists of discrete digital components but it can also use an inexpensive DSP. Operation is shown to be close to the MPP throughout a day-time period. The slight discrepancy is due to the inability of the controller to account for temperature variation.

The best fixed voltage algorithm (BFV): The control sets either the operating point of the PV array to the BFV or the output voltage to the nominal load voltage. Operation is therefore never exactly at the MPP and different data has to be collected for different geographical regions.

Linear reoriented coordinates method (*LRCM*): It requires the measurement of V_{OC} and I_{SC} to find the solution. Other constants representing the PV array characteristic curve are also needed. The maximum error in using LRCM to approximate the MPP was found to be 0.3%, but this was based only on simulation results.

Slide control method: Slide control method with a buck-boost converter is used to achieve MPPT. The switching function u of the converter is based on the fact that $dP/dV > 0$ on the left of the MPP and $dP/dV < 0$ on the right. This control was implemented using a microcontroller that senses the PV array voltage and current. The operation converges to the MPP in several tens of milliseconds.

The System Oscillation method: It is based on the principle of maximum power transfer and it uses the oscillations to determine the optimum point of operation. At the MPP the ratio of the amplitude of the oscillation and the average voltage is constant. This method requires only the sensing of the array voltage and its implementation is basically characterized by the use of filters. So, this method can be easily implemented with only analogical circuitries. Oscillation method is basically characterized by the use of filters [19].

The Ripple Correlation control (RCC): It is based on the principles of maximum power transfer and it uses the oscillations in power through all pass filters to obtain the optimal point. In other words, the high-frequency ripple in power and voltage is then captured using high-frequency filters, which are used to compute dP/dV. Then, the sign of this derivative is used in a signum function to indicate the right region of operation and an integrator also ensures the MPP.

RCC: It correlates the time derivative of the time-varying PV array power with the time derivative of the time-varying PV array current or voltage to drive the power gradient to zero, thus reaching the MPP. If the voltage or the current is increasing and the power is increasing, then the operating point is below the MPP ($V < V_{mpp}$ or $I < I_{mpp}$) as shown in Fig. 6 [44]. On the other hand, if v or i is increasing and p is decreasing, then the operating point is above the MPP ($V > V_{mpp}$ or $I > I_{mpp}$).

The three point weight comparison method: It is preferred to avoid having to move rapidly the operation point, when the solar radiation is varying quickly or when a disturbance or data reading error occur [56]. The algorithm of the three-point weight comparison is run periodically by perturbing the PV array terminal voltage and comparing its output power on current operation point (A), a point, B, perturbed from point A, and a point, C, with doubly perturbed in the opposite direction from point B of the *P–V* curve. In these cases, for points A and B, if the power of point B is greater than or equal to that of point A, the status is assigned a positive weighting. Otherwise, the status is assigned a negative weighting. And, for the points A and C, when the power of point C is smaller than that of point A, the status is assigned a positive weighting. Otherwise, the status is assigned a negative weighting. Of the three measured points, if two are positively weighted, the perturb direction should be kept same. On the contrary, when two are negatively weighted, the perturb direction should be reversed. In the other cases with one positive and one negative weighting, the MPP is reached and the voltage is not to be changed [96,97].

Array reconfiguration: In this system the PV arrays are arranged in different series and parallel combinations such that the resulting MPPs meet specific load requirements. This method is time consuming and tracking MPP in real time is not obvious [98].

Linear current control (LCC): It is used based on the fact that a linear relationship exists between *IMPP* and the level of irradiance [99]. The current I_{MPP} is thus found by sensing the irradiance level and a PI controller is used such that the PV array current follows I_{MPP}.

State-based MPPT: The system is represented by a state space model, and a nonlinear time varying dynamic feedback controller is used to track the MPP [100]. Simulations confirm that this technique is robust and insensitive to changes in system parameters and that MPPT is achieved even with changing atmospheric conditions and in the presence of multiple local maxima caused by partially shaded PV array or damaged cells. However, no experimental verification is given.

Look-up table method: In this case, the measured values of the PV generator's voltage and current are compared with those stored in the controlling system, which correspond to the operation at the maximum point, under predetermined climatologically conditions. In one of the methods I_{PV} is defined as a function of $P_{PV} \times IMPP = f(P_{max})$ [101]. In this method, a PI type controller adjusts the duty cycle of the dc–dc converter. The zero error is reached when the current and power of the photovoltaic generator are equal to the pre-determined values of IMPP and P_{max}. Any change of the insolation or load, results in a disturbance of the tuned system, and the PI controller again brings the system to its optimum operating point. These algorithms have the disadvantage that a large capacity of memory is required for storage of the data.

Variable inductor MPPT method: This method presents a new topology of MPPT controller for solar power applications that incorporated a variable inductance versus current characteristic. Power transfer in solar photovoltaic applications is achieved by impedance matching with a dc–dc converter with MPPT by the incremental conductance method. Regulation and dynamic control is achieved by operating with continuous conduction. It has been shown that under stable operation, the required output inductor has an inductance versus current characteristic whereby the inductance falls off with increasing current, corresponding to increasing incident solar radiation [102].

Variable step-size incremental resistance (INR) method: The step-size for the incremental conductance MPPT determines how fast the MPP is tracked. Fast tracking can be achieved with bigger increments, but the system might not run exactly at the MPP, instead oscillates around it; thus, there is a comparatively low efficiency. This situation is inverted when the MPPT is operating with a smaller increment. So a satisfying tradeoff between the dynamics and oscillations has to be made for the fixed step-size MPPT. The variable step size iteration can solve the tough design problem [103].

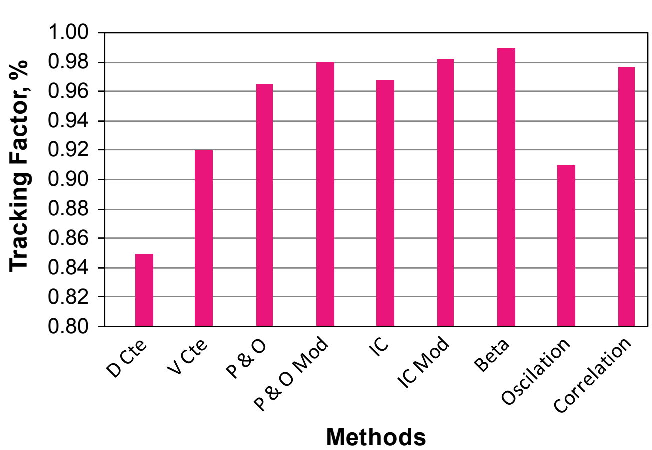


Fig. 35. Percent of energy extracted from PV panel. (adapted from [19])

Aiming to compare and adjust appropriately each algorithm according to the application it becomes necessary to provide performance measures that can be used for comparison criteria. Beyond the typical measures of dynamic responses, there are also additional metrics that may be used. Because the transmitted energy is essential for the use of PV as an energy source, a very important measure is the tracking factor, which is the percentage of available energy that was converted. The ripple voltage in steady state is also of vital importance, as there is a limit of ripple so that the panel will remain effectively at the MPP. Other factors such as ease of implementation, number of sensors and cost are also desirable. Fig. 35 shows the tracking factor versus different methods used to measure the performance. It is clear that P&O modified, IC modified, Ripple Correlation and Beta methods stands out. The Beta method can extract the greatest amount of energy from the PV and being in the order of 98.8% [19].

The major characteristics of different MPPT techniques that can be used for PV applications are summarized in Table 5 [44,104].

3. Grid connection in urban areas/microinverter requirements

Grid interconnection of PV power generation system has the advantage of more effective utilization of generated power.

Table 5
Major characteristics of different MPPT techniques [44,104].

MPPT technique	PV array dependent?	True MPPT?	Analog or digital?	Periodic tuning?	Convergence speed	Implementation complexity	Sensed parameters
Hill climbing/P&O	No	Yes	Both	No	Varies	Low	Voltage, current
Incremental conductance	No	Yes	Digital	No	Varies	Medium	Voltage, current
Fractional V_{OC}	Yes	No	Both	Yes	Medium	Low	Voltage
Fractional I_{SC}	Yes	No	Both	Yes	Medium	Medium	Current
Fuzzy logic control	Yes	Yes	Digital	Yes	Fast	High	Varies
Neural network	Yes	Yes	Digital	Yes	Fast	High	Varies
RCC	No	Yes	Analog	No	Fast	Low	Voltage, current
Current sweep	Yes	Yes	Digital	Yes	Slow	High	Voltage, current
dc Link capacitor droop control	No	No	Both	No	Medium	Low	Voltage
Load I or V maximization	No	No	Analog	No	Fast	Low	Voltage, current
dP/dV or dP/dI feedback control	No	Yes	Digital	No	Fast	Medium	Voltage, current
Array reconfiguration	Yes	No	Digital	Yes	Slow	High	Voltage, current
Linear current control	Yes	No	Digital	Yes	Fast	Medium	Irradiance
I_{MPP} and V_{MPP} computation	Yes	Yes	Digital	Yes	N/A	Medium	Irradiance, temperature
State based MPPT	Yes	Yes	Both	Yes	Fast	High	Voltage, current
OCC MPPT	Yes	No	Both	Yes	Fast	Medium	Current
BFV	Yes	No	Both	Yes	N/A	Low	None
LRCM	Yes	No	Digital	No	N/A	High	Voltage, current
Slide control	No	Yes	Digital	No	Fast	Medium	Voltage, current
β Method	No	Yes	Digital	No	Fast	High	Voltage, current
System oscillation method	No	Yes	Analog	No	N/A	Low	Voltage
Constant voltage tracker	Yes	No	Digital	Yes	Medium	Low	Voltage
Lookup table method	Yes	Yes	Digital	Yes	Fast	Medium	Voltage, current, Irradiance, temperature
Online MPP search algorithm	No	Yes	Digital	No	Fast	High	Voltage, current
Temperature method	No	Yes	Digital	Yes	Medium	High	Voltage, irradiance, Temperature
Three point weight comparison	No	Yes	Digital	No	Varies	Low	Voltage, current
POS control	No	Yes	Digital	No	N/A	Low	Current
Biological swarm chasing MPPT	No	Yes	Digital	No	Varies	High	Voltage, current, Irradiance, temperature
Variable inductor MPPT	No	Yes	Digital	No	Varies	Medium	Voltage, current
INR method	No	Yes	Digital	No	High	Medium	Voltage, current

However, the technical requirements from both the utility power system grid side and the PV system side need to be satisfied to ensure the safety of the PV installer and the reliability of the utility grid. Clarifying the technical requirements for grid interconnection and solving the problems such as islanding detection, harmonic distortion requirements and electromagnetic interference are therefore very important issues for widespread application of PV systems [105].

The electric grid has been designed for the traditional central generation, regional high voltage transmission and lower voltage customer-sited distribution. This design is for one-way power flow and has proven to be safe, reliable, and least cost. However, the paradigm is quickly changing due to price increases of traditional generation, price decreases of PV, policy drivers for PV and value shifts with awareness of climate change. Grid-connected PV is still a small portion of generation for most grids, but with 30% growth annually during the past decade and a potential doubling in 2008 [106], integration of PV into the traditional grid design will quickly become an issue.

The potential impacts and expected benefits of distributed PV grid interconnections are defined in [107]. The countermeasure technologies that may be applied to minimize the impacts as well as technologies that can enhance the benefits are summarized in Table 6. Details of each countermeasure technology, including application diagrams are provided in [107].

Generally, the penetration of PV on the grid is still small enough that grid operators are not experiencing issues [108,109]. However, it is difficult to directly apply the demonstration test outcomes to other areas because of inherent factors in each area (line length, demand characteristics, grid configurations, distribution capacities, PV inverter characteristics, and distribution of PV systems, among others) that greatly influence the impacts on grids.

The following characteristics should be referred to when contemplating the construction of future grid systems free of constraints on PV grid interconnections [107].

- Integrated system management using Information and Communication Technology (ICT).
- Extension of distribution capacities.
- Development and widespread use of storage technologies or integration of either grid load control or building load control with PV generation output.
- Provision of power quality that fits the corresponding application.

Microinverter solar systems require many inverters to handle a specific power level—driving up production quantities, which reduces cost [110].

- Maximum power point tracking (MPPT) algorithm is required to optimize the power harvest from solar panels.
- System efficiency: greater than 94%.
- Wide dc input voltage range.

Table 6
Summary of countermeasures [107].

	Countermeasures		
	Grid side	**Demand side**	**PV side**
Overvoltage/undervoltage	• Line voltage drop compensator • Shunt capacitor • Shunt reactor • Step voltage regulator • Electric storage devices	• Shunt capacitor • Shunt reactor • Electric storage devices	• Voltage control by PCS • Electric storage devices
Instantaneous voltage change (sags/swells)	• Thyristor voltage regulator • Static var compensator • Static synchronous compensator • Electric storage devices	• Dynamic voltage restorer • Electric storage devices	• Electric storage devices
Voltage imbalance	• Static var compensator	• Dynamic voltage restorer	
Harmonics shunt capacitor	• Shunt reactor • Static var compensator • Passive filter • Active filter	• Shunt capacitor • Shunt reactor • Dynamic voltage restorer • Passive filter • Active filter	• Advanced PCS
Unintended islanding protection	• Electric storage devices • Protective devices • Transfer trip equipment	• Electric storage devices • Protective devices	• Electric storage devices • Advanced PCS
Short-circuit capacity			• Advanced PCS
Disconnection time for intersystem fault	• Transfer trip equipment		
Increase in dc offset from PC			• Advanced PCS • dc Offset detector
Frequency fluctuation	• Electric storage devices	• Electric storage devices	• Electric storage devices
Supply security	• Electric storage devices	• Electric storage devices	• Electric storage devices
Peak cut electric storage devices	• Electric storage devices	• Electric storage devices	• Advanced PCS

- Cost per Watt: $0.20–$0.50 USD in production quantities.
- Safety: fault detection and anti-islanding.
- ac Quality, total harmonic distortion (THD) $<5\%$: meets IEEE 519 standard.

A general structure of a grid-connected solar microinverter system is shown in Fig. 36.

Fig. 37 shows the system block diagram of grid-connected solar microinverter reference design that controlled by a single dsPIC DSC device. The dsPIC DSC device is the heart of the Solar Microinverter design and controls all critical operations of the system as well as the housekeeping operations. Due to the life span of a PV panel, which is typically 25 years, two key requirements of the solar microinverter reference design are high efficiency and reliability. The functions of the dsPIC DSC can be broadly classified into the following categories [110]:

- All power conversion algorithms.
- Inverter state machine for the different modes of operation.
- Maximum power point tracking (MPPT).

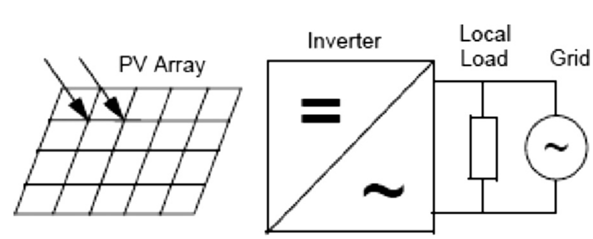


Fig. 36. Grid-connected solar microinverter system.

- Digital phase-locked loop (PLL).
- System islanding and fault handling.

The dsPIC DSC device offers intelligent power peripherals specifically designed for power conversion applications.

These intelligent power peripherals include the high-speed PWM, high-speed 10-bit ADC, and high-speed analog comparator modules. These peripheral modules include features that ease the

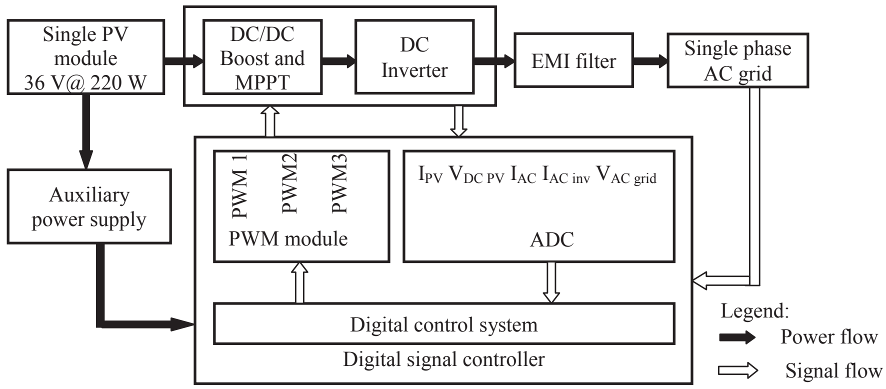


Fig. 37. Grid-connected solar microinverter block diagram [110].

control of any switch mode power supply with a high-resolution PWM, flexible ADC triggering, and comparator fault handling.

4. Conclusion

Efficient energy use not only saves fossil fuels and energy, but also brings financial advantages. Providing energy efficient solutions can help to resolve some of energy problems. The use of energy from photovoltaic panels is a reality, and its intensive use will very soon become extremely important in finding solutions to energy and environmental problems. Energy efficiency concerns the entire chain of energy conversion—from effective generation to transmission and distribution of electrical energy to economical use. The output power delivered by a PV module can be maximized using MPPT control system. It consists of a power conditioner to interface the PV output to the load, and a control unit, which drives the power conditioner for extracting the maximum power from a PV array. Several MPPT techniques taken from the literature are discussed herein, with their pros and cons. There are some MPPT able to reach the global maximum power point under partial shading conditions. The grid interconnection of PV power generation system and solar microinverter requirements are discussed. Among the methods investigated, Beta was presented as an excellent solution regarding the best amount of energy extracted (tracking factor), reduced and smaller ripple voltage in steady state, good transient performance and simplicity of implementation, resulting in best overall performance among the investigated techniques. Also, the Ripple Correlation, modified IC and P&O, could be an alternative for high quality performance for the MPPT algorithms. Microinverter solar systems require many inverters to handle a specific power level—driving up production quantities, which reduces cost. The concluding discussion and table may serve as a useful guide in choosing the right MPPT method for specific PV systems.

References

[1] Bhubaneswari P, Iniyan S, Goic R. A review of solar photovoltaic technologies. Renewable and Sustainable Energy Reviews 2011;15:1625–36.
[2] Baltas P, Tortoreli M, Russell PE. Evaluation of power output for fixed and step tracking photovoltaic arrays. Solar Energy 1986;37(2):147–63.
[3] Chander M, Chopra KL, Joshi JC, Mukerjee AK. Comparative study of different orientations of photovoltaic system. Solar & Wind Technology 1988;5 (3):329–34.
[4] Ramamurthy V, Tiku P, Radhamohan V, Rao MVB. Evaluation of outdoor performance of polycrystalline silicon photovoltaic panel. In: Proceedings of 6th international photovoltaic science and engineering conference, New Delhi, February 10–14; 1992. p. 917–23.
[5] Snyman DB, Enslin HR. Novel technique for improved power conversion efficiency in systems with battery back-up. Renewable Energy 1994;4(3):349–57.
[6] de Brito MAG, Sampaio LP, Junior LG, Canesin CA. Evaluation of MPPT techniques for photovoltaic applications. In: Proceedings of the industrial electronics (ISIE) 2011 IEEE international symposium; 2011. p. 1039–44.
[7] Hsieh GC, et al. Variable frequency controlled incremental conductance derived MPPT photovoltaic stand-along dc bus system. In: Proceedings of APEC, vol. 23; 2008. p. 1849–54.
[8] Kwon JM, et al. Photovoltaic power conditioning system with line connection. IEEE Transactions on Industrial Electronics, New York 2006;53(5):1048–54.
[9] Yu WL, et al. A dsp-based single-stage maximum power point tracking PV inverter. In: Proceedings of APEC, vol. 25; 2010. p. 948–52.
[10] Pandey A, et al. A simple single-sensor MPPT solution. IEEE Transactions on Power Electronics, New York 2007;22(6):698–700.
[11] Casadei D, et al. Single-phase single-stage photovoltaic generation system based on a ripple correlation control maximum power point tracking. IEEE Transactions on Energy Conversion 2006;21(2):562–8.
[12] Li W, et al. A smart and simple PV charger for portable applications. In: Proceedings of APEC, vol. 25, p. 2080–4; 2010.
[13] Jain S, Agarwal V. A new algorithm for rapid tracking of approximate maximum power point in photovoltaic systems. IEEE Power Electronics Letters 2004;2(1):16–9.
[14] Ho BMT, et al. Use of system oscillation to locate the MPP of PV panels. IEEE Power Electronics Letters 2004;2(1):1–5.
[15] Hasan KN, et al. An improved maximum power point tracking technique for the photovoltaic module with current mode control. In: Proceedings of AUPEC, vol. 19; 2009. p. 1–6.
[16] Altas IH, Sharaf AM. A solar powered permanent magnet DC motor drive scheme. In: Proceedings of the 17th annual conference of solar energy society of Canada, Toronto, Ontario, Canada; 1991. p. 65–7.
[17] Sharaf AM, Wang L. A photovoltaic powered efficient DC motor drive for pump irrigation. In: Proceedings of the Canadian solar energy conference, Halifax, N.S., Canada; 1990.
[18] Hohm DP, Ropp ME. Comparative study of maximum power point tracking algorithms. Progress in Photovoltaics: Research and Applications 2003;11:47–62, http://dx.doi.org/10.1002/pip.459.
[19] de Brito MAG., Sampaio LP, Luigi G, E Melo GA, Canesin CA. Comparative analysis of MPPT techniques for PV applications. In: Proceedings of 2011 international conference on clean electrical power (ICCEP); 2011. p. 99–104.
[20] Teulings WJA, Marpinard JC, Capel A, O'Sullivan D. A new maximum power point tracking system. In: Proceedings 24th annual IEEE power electronics specialists conference; 1993. p. 833–8.
[21] Kim Y, Jo H, Kim D. A new peak power tracker for cost-effective photovoltaic power system. In: Proceedings of 31st intersociety energy conversion engineering conference; 1996. p. 1673–8.
[22] Hashimoto O, Shimizu T, Kimura G. A novel high performance utility interactive photovoltaic inverter system. In: Proceedings of conference record of 2000 IEEE industry applications conference; 2000. p. 2255–60.
[23] Koutroulis E, Kalaitzakis K, Voulgaris NC. Development of a microcontroller-based, photovoltaic maximum power point tracking control system. IEEE Transactions on Power Electronics 2001;16(21):46–54.
[24] Veerachary M, Senjyu T, Uezato K. Maximum power point tracking control of IDB converter supplied PV system. In: IEE proceedings of electric power applications; 2001. p. 494–502.
[25] Xiao W, Dunford WG. A modified adaptive hill climbing MPPT method for photovoltaic power systems. In: Proceedings of 35th annual IEEE power electronics specialists conference; 2004. p. 1957–63.
[26] Wasynczuk O. Dynamic behavior of a class of photovoltaic power systems. IEEE Transactions on Power Apparatus and Systems 1983;102(9):3031–7.
[27] Hua C, Lin JR. DSP-based controller application in battery storage of photovoltaic system. In: Proceedings of IEEE IECON 22nd international conference on industrial electronics, control and instrumentation; 1996. p. 1705–10.
[28] Slonim MA, Rahovich LM. Maximum power point regulator for 4 kW solar cell array connected through invertor to the ac grid. In: Proceedings of 31st intersociety energy conversion engineering conference; 1996. p. 1669–72.

[29] Al-Amoudi A, Zhang L. Optimal control of a grid-connected PV system for maximum power point tracking and unity power factor. In: Proceedings of the seventh international conference on power electronics and variable speed drives; 1998. p. 80–5.
[30] Kasa N, Iida T, Iwamoto H. Maximum power point tracking with capacitor identifier for photovoltaic power system. In: Proceedings of the eighth international conference on power electronics and variable speed drives; 2000. p. 130–5.
[31] Zhang L, Al-Amoudi A, Bai Y. Real-time maximum power point tracking for grid-connected photovoltaic systems. In: Proceedings of the eighth international conference on power electronics and variable speed drives; 2000. p. 124–9.
[32] Hua CC, Lin JR. Fully digital control of distributed photovoltaic power systems. In: Proceedings of IEEE symposium on industrial electronics; 2001. p. 1–6.
[33] Femia N, Petrone G, Spagnuolo G, Vitelli M. Optimization of perturb and observe maximum power point tracking method. IEEE Transactions on Power Electronics 2005;20(4):963–73.
[34] Wolfs PJ, Tang L. A single cell maximum power point tracking converter without a current sensor for high performance vehicle solar arrays. In: Proceedings of 36th annual IEEE power electronics specialists conference; 2005. p. 165–71.
[35] D'Souza NS, Lopes LAC, Liu X. An intelligent maximum power point tracker using peak current control. In: Proceedings of 36th annual IEEE power electronics specialists conference; 2005. p. 172–7.
[36] Kasa N, Iida T, Chen L. Flyback inverter controlled by sensorless current MPPT for photovoltaic power system. IEEE Transactions on Industrial Electronics 2005;52(4):1145–52.
[37] Youngseok J, et al. Improved perturbation and observation method (IP&O) of MPPT control for photovoltaic power systems. In: Proceedings of 31st IEEE photovoltaic specialists conference; 2005.
[38] Chee Wei T, Green TC, Hernandez-Aramburo CA. A current mode controlled maximum power point tracking converter for building integrated photovoltaics. In: Proceedings of European conference on power electronics and applications; 2007.
[39] Al-Diab A, Sourkounis C. Variable step size P&O MPPT algorithm for PV systems. In: Proceedings of optimization of electrical and electronic equipment (OPTIM) conference; 2010.
[40] Fangrui L, et al. A variable step size INC MPPT method for PV systems. IEEE Transactions on Industrial Electronics 2008;55(7):2622–8.
[41] Marcelo Gradella Villalva JRG, Ernesto Ruppert Filho. Analysis and simulation of the P&O Algorithm Using A Linearized PV array model. In: Proceedings of industrial electronics conference, IECON' 09; 2009. p. 231–6.
[42] Mei Shan Ngan, Chee Wei Tan. A study of maximum power point tracking algorithms for stand-alone photovoltaic systems. In: Proceedings of 2011 IEEE applied power electronics colloquium (IAPEC); 2011. p. 22–7.
[43] Enslin JHR, Wolf M, Swiegers W. Integrated photovoltaic maximum power point tracking converter. IEEE Transactions on Industrial Electronics 1997;44(6):769–73.
[44] Esram T, Chapman PL. Comparison of photovoltaic array maximum power point tracking techniques. IEEE Transactions on Energy Conversion 2007;22(2):439–49.
[45] Tafticht T, Agbossou K. Development of a MPPT method for photovoltaic systems. In: Canadian conference on electrical and computer engineering; 2004. p. 1123–6.
[46] Hsiao YT, Chen CH. Maximum power tracking for photovoltaic power system. In: Proceedings of the conference record of 37th IAS annual meeting industry applications conference; 2002. p. 1035–40.
[47] Hussein KH, Zhao G. Maximum photovoltaic power tracking: an algorithm for rapidly changing atmospheric conditions. IEE Proceedings of Generation, Transmission, Distribution 1995;142(1):59–64.
[48] Wu W, Pongratananukul N, Qiu W, Rustom K, Kasparis T, Batarseh I. DSP-based multiple peak power tracking for expandable power system. In: Proceedings of the eighteenth annual applied power electronics conference and exposition; 2003. p. 525–30.
[49] Kobayashi K, Takano I, Sawada Y. A study on a two stage maximum power point tracking control of a photovoltaic system under partially shaded insolation conditions. In: Proceedings of IEEE power engineering society general meeting; 2003. p. 2612–7.
[50] Salameh Z, Dagher F, Lynch W. Step-down maximum power point tracker for photovoltaic systems. Solar Energy 1991;46(5):279–82.
[51] Buresch M. Photovoltaic energy systems. New York: McGraw Hill; 1983.
[52] Masoum MAS, Dehbonei H, Fuchs EF. Theoretical and experimental analyses of photovoltaic systems with voltage and current-based maximum power-point tracking. IEEE Transactions on Energy Conversion 2002;17(4):514–22.
[53] Noh HJ, Lee DY, Hyun DS. An improved MPPT converter with current compensation method for small scaled PV-applications. In: Proceedings of 28th annual conference of the IEEE industrial electronics society; 2002. p. 1113–8.
[54] Kobayashi K, Matsuo H, Sekine Y. A novel optimum operating point tracker of the solar cell power supply system. In: Proceedings of 35th annual IEEE power electronics specialists conference; 2004. p. 2147–51.
[55] Bekker B, Beukes HJ. Finding an optimal PV panel maximum power point tracking method. In: Proceedings of 7th AFRICON conference, Africa; 2004. p. 1125–9.
[56] Sayal A. MPPT techniques for photovoltaic system under uniform insolation and partial shading conditions. In: Proceedings of 2012 students conference on engineering and systems (SCES); 2012. p. 1–6.
[57] Hart GW, Branz HM, Cox CH. Experimental tests of open loop maximum-power-point tracking techniques. Solar Cells 1984;13:185–95.
[58] Yuvarajan S, Xu S. Photo-voltaic power converter with a simple maximum-power-point-tracker. In: Proceedings of 2003 International Symposium on Circuits and Systems; 2003. p. III-399–402.
[59] Krisztina Leban, Ewen RitchieAalborg. Selecting the accurate solar panel simulation model. Nordic workshop on power and industrial electronics; 2008.
[60] Brambilla A, et al. New approach to photovoltaic arrays maximum power point tracking. Proceedings of the 30th IEEE power electronics conference; 1998. 632–7.
[61] Matsui M, Kitano T, Xu DH, Yang ZQ. A new maximum photovoltaic power tracking control scheme based on power equilibrium at DC link. In: Proceedings of conference record of 1999 IEEE industry applications conference; 1999. p. 804–9.
[62] Kitano T, Matsui M, Xu DH. Power sensor-less MPPT control scheme utilizing power balance at DC link-system design to ensure stability and response. In: Proceedings of 27th IEEE industrial electronics society annual conference; 2001. p. 1309–14.
[63] Itako K, Mori T. A current sensorless MPPT control method for a stand-alone-type PV generation system. Electrical Engineering in Japan 2006;157(2).
[64] Mohan N, Undel TM, Robbins WP. Power electronics: converters, applications, and design. Hoboken (NJ): Wiley; 2004.
[65] Zue AO, Chandra A. Simulation and stability analysis of a 100 kW grid-connected LCL photovoltaic inverter for industry. In: Proceedings of IEEE power engineering society general; June 2006. p.1–6.
[66] Bhide R, Bhat SR. Modular power conditioning unit for photovoltaic applications. In: Proceedings of 23rd annual IEEE power electronics specialists conference; 1992. p. 708–13.
[67] Hou CL, Wu J, Zhang M, Yang JM, Li JP. Application of adaptive algorithm of solar cell battery charger. In: Proceedings of IEEE international conference on electric utility deregulation and restructuring and power technologies; 2004. p. 810–3.
[68] Kuo YC. Design and implementation of single stage photovoltaic energy conversion system [Ph.D. dissertation]. Department of Electrical engineering, National Cheng Kung University Tainan, Taiwan, R.O.C.; 2001.
[69] IEEE Recommended Practice for Utility. Interface of photovoltaic (PV) systems, IEEE standard 929-2000; January 2000.
[70] Bleijs JAM, Gow A. Fast maximum power point control of current-fed DC–DC converter for photovoltaic arrays. Electronics Letters 2001;37:5–6.
[71] Zhou D, Zhengming Z, Eltawil M, Yuan L. Design and control of a three-phase grid-connected photovoltaic system with developed maximum power point tracking. In: Proceedings of the twenty-third annual IEEE applied power electronics conference and exposition (APEC), February 24–28; 2008. p. 973–9.
[72] Won CY, Kim DH, Kim SC, Kim WS, Kim HS. A new maximum power point tracker of photovoltaic arrays using fuzzy controller. In: Proceedings of 25th annual IEEE power electronics specialists conference; 1994. p. 396–403.
[73] Simoes MG, Franceschetti NN, Friedhofer M. A fuzzy logic based photovoltaic peak power tracking control. In: Proceedings of IEEE international symposium on industrial electronics; 1998. p. 300–5.
[74] Mahmoud AMA., Mashaly HM, Kandil SA, El Khashab H, Nashed MNF. Fuzzy logic implementation for photovoltaic maximum power tracking. In: Proceedings of 9th IEEE international workshop robot human interactive communication; 2000. p. 155–60.
[75] Patcharaprakiti N, Premrudeepreechacharn S. Maximum power point tracking using adaptive fuzzy logic control for grid-connected photovoltaic system. In: Proceedings of IEEE power engineering society winter meeting; 2002. p. 372–7.
[76] Veerachary M, Senjyu T, Uezato K. Neural-network-based maximum-power-point tracking of coupled-inductor interleaved-boostconverter-supplied PV system using fuzzy controller. IEEE Transactions on Industrial Electronics 2003;50(4):749–58.
[77] Khaehintung N, Pramotung K, Tuvirat B, Sirisuk P. RISC-microcontroller built-in fuzzy logic controller of maximum power point tracking for solar-powered light-flasher applications. In: Proceedings of 30th annual conference of the IEEE industrial electronics society; 2004. p. 2673–8.
[78] Bouchafaa F, Boucherit MS. Modeling and Simulation of a gird connected PV generation system with MPPT fuzzy logic control. In: Proceedings of 7th international multi-conference on systems on signals and devices; 2010.
[79] Subiyanto Hannan MA. Maximum Power Point Tracking in Grid Connected PV system using a novel fuzzy logic controller. In: Proceedings of IEEE student conference on research and development; 2009.
[80] Harada J, Zhao G. Controlled power-interface between solar cells and ac sources. In: Proceedings of IEEE telecommunications power conference; 1989. p. 22.1/1–7.
[81] Alajmi BN, Khaled HA, Stephen JF, Barry WW. A maximum power point tracking technique for partially shaded photovoltaic systems in microgrids. IEEE Transactions on Industrial Electronics 2013;60(6):1596–606.
[82] Kislovski AS, Redl R. Maximum-power-tracking using positive feedback. In: Proceedings 25th annual IEEE power electronics specialists conference; 1994. p. 1065–8.

[83] Shmilovitz D. On the control of photovoltaic maximum power point tracker via output parameters. In: IEE proceedings of electric power applications; 2005. p. 239–48.
[84] Hiyama T, Kouzuma S, Imakubo T. Identification of optimal operating point of PV modules using neural network for real time maximum power tracking control. IEEE Transactions on Energy Conversion 1995;10(2):360–7.
[85] Ro K, Rahman S. Two-loop controller for maximizing performance of a grid-connected photovoltaic-fuel cell hybrid power plant. IEEE Transactions on Energy Conversion 1998;13(3):276–81.
[86] Hussein A, Hirasawa K, Hu J, Murata J. The dynamic performance of photovoltaic supplied dc motor fed from DC–DC converter and controlled by neural networks. In: Proceedings of international joint conference neural network; 2002. p. 607–12.
[87] Zhang L, Bai Y, Al-Amoudi A. GA-RBF neural network based maximum power point tracking for grid-connected photovoltaic systems. In: Proceedings of international conference on power electronics, machines and drives; 2002. p. 18–23.
[88] Weidong Xiao, Elnosh A, Khadkikar V, Zeineldin H. Overview of maximum power point tracking technologies for photovoltaic power systems. In: Proceedings of IECON 2011—37th annual conference on IEEE industrial electronics society; 2011. p. 3900–5.
[89] Chen YM, et al. Multiinput converter with power factor correction, maximum power point tracking, and ripple-free input currents. IEEE Transactions on Power Electronics 2004;19:631–9.
[90] Wanzeller MG, et al. Current control loop for tracking of maximum power point supplied for photovoltaic array. IEEE Transactions on Instrumentation and Measurement 2004;53:1304–10.
[91] Masoum MA, et al. Theoretical and experimental analyses of photovoltaic systems with voltage and current-based maximum power point tracking. Power Engineering Review, IEEE 2002;22:62.
[92] Xiao W, et al. Topology study of photovoltaic interface for maximum power point tracking. IEEE Transactions on Industrial Electronics 2007;54:1696–704.
[93] Xiao W, et al. Regulation of photovoltaic voltage. IEEE Transactions on Industrial Electronics 2007;54:1365–74.
[94] Casadei D, et al. Single-phase single-stage photovoltaic generation system based on a ripple correlation control maximum power point tracking. IEEE Transactions on Energy Conversion 2006;21:562–8.
[95] Koizumi H, et al. A novel microcontroller for grid-connected photovoltaic systems. IEEE Transactions on Industrial Electronics 2006;53:1889–97.
[96] Yafaoui WU, Cheung R. Implementation of maximum power point tracking algorithm for residential photovoltaic systems. In: Proceedings of 2nd Canadian solar buildings conference calgary; 2007.
[97] Durgadevi SA, Natarajan SP. Study and implementation of maximum power point tracking (MPPT) algorithm for photovoltaic systems. In: Proceedings of 1st international conference on electrical energy systems (ICEES); 2011.
[98] El-Shibini MA, Rakha HH. Maximum power point tracking technique. In: Proceedings of electrotechnical conference on integrating research, industry and education in energy and communication engineering; 1989. p. 21–4.
[99] Pan CT, Chen JY, Chu CP, Huang YS. A fast maximum power point tracker for photovoltaic power systems. In: Proceedings of 25th annual conference of the IEEE industrial electronics society; 1999. p. 390–3.
[100] Solodovnik EV, Liu S, Dougal RA. Power controller design for maximum power tracking in solar installations. IEEE Transactions on Power Electronics 2004;19(5):1295–304.
[101] Desai HP, Patel HK. Maximum power point algorithm in PV generation: an overview. In: Proceedings of 7th international conference on power electronics and drive systems 2007, PEDS '07; 2007. p. 624–30.
[102] Zhang L, Hurley WG, Wolfle W. A new approach to achieve maximum power point tracking for PV system with a variable inductor. In: Proceedings of 2nd IEEE international symposium on power electronics for distributed generation systems; 2010. p. 948–52.
[103] Mei Q, Shan M, Liu L, Guerrero JM. A novel improved variable step-size incremental resistance (INR) MPPT method for PV systems. IEEE; 2010. p. 242–2434.
[104] Ali ANA, Saied MH, Mostafa MZ, Abdel-Moneim TM. A survey of maximum PPT techniques of PV systems; 2012. p. 1–17.
[105] Ishikawa T. Grid-connected photovoltaic power systems: survey of inverter and related protection equipments. Report IEA (International Energy Agency) PVPS T5-05; 2002 ⟨http://www.iea-pvps.org⟩.
[106] DISPOWER Project. Summary report on impact of power generators distributed in low voltage grid segments; 2005 ⟨http://www.dispower.org⟩.
[107] IEA PVPS Task 10. Overcoming PV grid issues in urban areas. Activity 3.3 Report IEA-PVPS T10-06; October 2009.
[108] PV Upscale. Impact of photovoltaic generation on power quality in urban areas with high PV population; 2008 ⟨http://www.pvupscale.org/IMG/pdf/WP4_D4-3_public_v1c.pdf⟩.
[109] PV Upscale. Recommendations for Utilities; 2008 ⟨http://www.pvupscale.org/IMG/pdf/WP4_D4-4_recommendations_V6.pdf⟩.
[110] AN1338. Grid-connected solar microinverter reference design using a dsPIC® digital signal controller. Microchip Technology Inc. 2010–2011; 2008 ⟨http://ww1.microchip.com/downloads/en/AppNotes/01338D.pdf⟩.